Published in final edited form as:

Nature. 2020 October ; 586(7827): 145–150. doi:10.1038/s41586-020-2761-3.

Synthetic group A streptogramin antibiotics that overcome Vat resistance

Qi Li[*,1], **Jenna Pellegrino**[*,2], **D. John Lee**[2], **Arthur A. Tran**[1], **Hector A. Chaires**[2], **Ruoxi Wang**[1], **Jesslyn E. Park**[2], **Kaijie Ji**[1], **David Chow**[1], **Na Zhang**[1,3], **Axel F. Brilot**[4], **Justin T. Biel**[2], **Gydo van Zundert**[5], **Kenneth Borrelli**[4], **Dean Shinabarger**[6], **Cindy Wolfe**[6], **Beverly Murray**[6], **Matthew P. Jacobson**[1], **Estelle Mühle**[7], **Olivier Chesneau**[7], **James S. Fraser**[2], **Ian B. Seiple**[1,#]

[1]-Department of Pharmaceutical Chemistry and Cardiovascular Research Institute, University of California, San Francisco, San Francisco, United States

[2]-Department of Bioengineering and Therapeutic Sciences, University of California, San Francisco, San Francisco, United States

[3]-College of Life Science and Bioengineering, Beijing University of Technology, Beijing 100124, China

[4]-Department of Biochemistry and Biophysics and Howard Hughes Medical Institute, University of California, San Francisco, San Francisco, United States

[5]-Schrödinger, New York, New York, United States

[6]-Micromyx, Kalamazoo, Michigan, United States

[7]-Collection de l'Institut Pasteur (CIP), Microbiology Department, Institut Pasteur, Paris, France

Abstract

[#]-correspondence to ian.seiple@ucsf.edu.

[*]-these authors contributed equally

Author Contributions

Q.L. and I.B.S. determined analogues for synthesis and designed the synthetic routes; Q.L. executed and optimized the syntheses of analogues, with assistance from A.A.T. (analogues 29–32), R.W. (analogue 21), K.J. (analogues 27 and 28), and D.C. (analogue 26); J.P. and D.J.L. prepared samples and collected cryo-EM data; J.P. and A.F.B. calculated cryo-EM reconstructions; J.P. and J.E.P. performed the VatA acetylation assay; J.P. performed the *in vitro* translation experiments; G.v.Z. and K.B. developed new tools for cryo-EM model refinement; J.P., K.B., and J.T.B. performed cryo-EM model refinements; G.v.Z., J.P., H.A.C., N.Z., and M.P.J. determined relative energies of macrocycle confirmations; H.A.C. collected X-ray crystallographic data and performed X-ray model refinements; D.S., C.W., B.M., E.M., and O.C. designed and executed the MIC assays; Q.L., J.P., I.B.S., and J.S.F. wrote the manuscript. All authors discussed the results and commented on the manuscript.

Competing Interests

K.B. and G.v.Z. are employees of Schrodinger Inc. D.S., C.W., B.M. are employees of Micromyx.

Code Availability

Forcefield-based refinement is available in PHENIX (versions 1.15 and later) using beta features available in Schrödinger 2019–3. Python code for analyzing IVT data and VatA kinetics data are available on github: https://github.com/fraser-lab/streptogramin

Data Availability

Models and maps generated during this study are available in the EMDB and PDB (accessions are listed in Tables 1 and 2). We plan to upload all raw data to EMPIAR.

Natural products serve as chemical blueprints for the majority of antibiotics in our clinical arsenal. The evolutionary process by which these molecules arise is inherently accompanied by the co-evolution of resistance mechanisms that shorten the clinical lifetime of any given class[1]. Virginiamycin acetyltransferases (Vats) are resistance proteins that provide protection against streptogramins[2], potent Gram-positive antibiotics that inhibit the bacterial ribosome[3]. Due to the challenge of selectively modifying the chemically complex, 23-membered macrocyclic scaffold of group A streptogramins, analogs that overcome Vat resistance have not been previously accessed[2]. Here we report the design, synthesis, and antibacterial evaluation of group A streptogramin antibiotics with unprecedented structural variability. Using cryo-electron microscopy and forcefield-based refinement, we characterize the binding of eight analogs to the bacterial ribosome at high resolution, revealing new binding interactions that extend into the peptidyl tRNA binding site and towards synergistic binders that occupy the nascent peptide exit tunnel (NPET). One of these analogs has excellent activity against several streptogramin-resistant strains of *S. aureus*, exhibits decreased acetylation rates *in vitro*, and is effective at lowering bacterial load in a mouse model of infection. Our results demonstrate that the combination of rational design and modular chemical synthesis can revitalize classes of antibiotics that are limited by naturally arising resistance mechanisms.

Natural antibiotics and semisynthesis

Natural product antibiotics often have poor characteristics as therapeutics[1] and are subject to resistance mechanisms that have arisen through coevolution[4]. A primary method to improve natural antibiotics for human use is semisynthesis: chemical modification of natural products obtained by biological production. This method has improved the pharmacological properties of many natural product classes, but has only achieved limited success in overcoming resistance[1]. Recently, advances in chemistry have enabled access to several antibiotic classes by fully synthetic routes that provide renewed avenues to overcome resistance[5,6].

Streptogramin antibiotics comprise two structurally distinct groups (A and B, Extended Data Figure 1a)[3] that act synergistically to achieve bactericidal activity in many organisms[7] by inhibiting the bacterial ribosome[8]. Group A binds to the peptidyl transferase center (PTC) and increases affinity for the group B component in the adjacent NPET[9]. Resistance to the A component mediates high-level resistance to the combination, whereas resistance to the B component results in intermediate resistance[10]. Like other PTC-targeting antibiotics, resistance to group A streptogramins can be mediated by ABC-F-family proteins that dislodge antibiotics[11] or Cfr methylases that methylate A2503 of the 23S RNA to sterically block binding[12]. A specific resistance mechanism for group A streptogramins is deactivation by virginiamycin acetyltransferases (Vats)[2]. These proteins acetylate the C14 alcohol, resulting in steric interference and disruption of a crucial hydrogen bond. The combination of *vat*(A) and *vgb*(A) genes (which deactivate the B component) is the most clinically relevant streptogramin resistance genotype in *S. aureus* in France, where streptogramins (under the trade name Pyostacine) are used orally for skin and soft tissue infections[13,14] as well as bone and joint infections[15]. Semisynthesis has improved water solubility (e.g., Synercid[16]) and increased potency (e.g., NXL-103[17]), but methods to overcome resistance to

the class have yet to be discovered. We[18,19] and others[20–28] have developed fully synthetic routes to group A streptogramins, but these routes have not been applied to the synthesis of novel analogs. Herein we report optimization of our initially reported route[18] and its application to the synthesis of analogs designed to overcome streptogramin resistance.

Structure-guided rational design

We hypothesized that group A streptogramins could be engineered to avoid Vat acetylation while maintaining or improving ribosomal binding (Extended Data Figure 1). We selected the natural product virginiamycin M2 (**VM2**) as our parent scaffold due to its ability to be converted to more active analogs (e.g., flopristin, **4**) by C16 fluorination[17]. To guide analog design (maintaining ribosomal activity while overcoming Vat binding), we obtained a 2.5-Å resolution cryo-electron microscopy (cryo-EM) structure of fully synthetic **VM2** bound to the *E. coli* 50S ribosome. Both the quality of the density, enabled by the advantageous properties of the ribosome as a cryo-EM sample, and the model, enabled by the forcefield-guided refinement[29,30], directed our analog design. We found that the binding determinants agreed with co-crystallographic data for other related group A streptogramins bound to bacterial[9,31,32] and archeal[33,34] ribosomes.

In the ribosome, the C3 isopropyl group on **VM2** participates in hydrophobic interactions with the face of U2585, but otherwise lacks binding interactions, suggesting that C3 modifications would be tolerated. Similarly, the C4 methyl group does not appear to make binding interactions and is angled towards the group B streptogramin binding site. In contrast, mutagenesis and crystallography of the resistance enzyme VatA identified key interactions between these groups (C3 isopropyl, C4 methyl, and C6 proton) and binding site residues necessary for acetylation[2]. Structural modifications of these positions might disrupt VatA binding and overcome Vat resistance, but only one semisynthetic streptogramin with modifications at one of these locations has been reported (hydrogenation of the C5-C6 alkene)[2,35]. Broader semisynthetic modifications of these positions are restricted by the lack of functional groups for chemoselective activation.

Modular synthesis of structural analogs

To directly test the hypothesis that C3 and C4 structural modifications could overcome Vat-based antibiotic resistance, we first developed a pipeline for the synthesis of group A streptogramins with unprecedented structural diversity. Our route to group A streptogramins (e.g., **VM2** in Figure 1a) comprises the convergent assembly of seven simple, individually diversifiable chemical building blocks[18]. We synthesize two halves of similar complexity, join them by amide bond coupling, and accomplish macrocyclization by means of a Stille cross-coupling reaction. Overall, the route is seven linear steps (11 total steps) from the starting building blocks, facilitating rapid generation of analogs. Importantly, the syntheses of the halves are highly scalable. By pooling decagram quantities of each, we can rapidly synthesize analogs with modifications on the complimentary half without repeating the entire synthesis. The route depicted in Figure 1a features technical improvements that increase yield through both the left half sequence (31% → 40%) and the right half sequence (18% → 28%) compared to our original report[18].

We were readily able to prepare 18 streptogramins by building block variation, including the natural products **VM2**, **VM1**, madumycin I (**33**), and madumycin II (**34**, Figure 1b). The template synthesis of **VM2** was used directly or with trivial modifications (e.g., a deprotection step) in most cases to deliver analogs in good yield (10–40% overall). For certain analogs, efficiency was impacted by functional group incompatibilities with the chemistry for assembly and modified route was required (see Supporting Information for details).

The incorporation of modified building blocks represents an effective approach to access novel analogs, but the diversity of our library is further enhanced by incorporating functional handles for late-stage diversification. Replacement of isobutyraldehyde (**7**) with para-methoxybenzyl-protected (*R*)- or (*S*)-3-hydroxy-2-methylpropanal in the left half sequence enabled access to C3-isopropyl-modified analogs **38** and **39** (Figure 1c, >1 g of each prepared). Each of these alcohol-appended streptogramins was allowed to react with 17 commercially available arylisocyanates, resulting in 34 novel streptogramin analogs with arylcarbamate side chains at the C3 position (**40a-q** and **41a-q**). The alcohols in **38** and **39** also served as effective precursors for the installation of secondary amines by oxidation/reductive amination (**42-44**, Figure 1d) and for incorporation of fluorine by treatment with diethylaminosulfur trifluoride. Additionally, we installedl fluorine at C16 by a 4-step sequence, providing the clinical candidate flopristin (**4**) and several fluorinated analogs (Figure 1e).

In vitro and *in vivo* efficacy

We evaluated the activity of 62 new group A streptogramin analogs (Extended Data Figure 2), four natural products, and the first fully synthetic sample of flopristin (**4**) against a 20 pathogen panel (Figure 2a and Extended Data Figures 3 **and** 4), including three strains with known mechanisms of streptogramin resistance (VatA and Cfr in *S. aureus*, ABC-F in *E. faecalis*). We also measured *in vitro* ribosomal translation inhibitory activities for selected analogs (blue bars on right, Figure 2a). Installation of a methyl group at C9 (**23**) or removal of the C12 methyl group (**24**) resulted in loss of activity. The latter result may provide biological rationale for the four additional biosynthetic steps required for its installation[36]. Introduction of a primary or tertiary amine (**32** and **42**, respectively) resulted in complete loss of activity, but interestingly, **42** inhibited translation *in vitro* as effectively as **VM2**. The poor cellular activity likely results from decreased entry or increased efflux, highlighting the challenge of designing antibiotics with both high on-target activity and high cellular accumulation[37]. Analogs **26**, **40q**, and **21** displayed equal or improved activity against WT and VatA *S. aureus* compared to **VM2**, and their C16-fluorinated homologues (**45**, **46**, and **47**) exhibited substantially improved activity. Notably, analogs **46** and **47** were 16- to 32-fold more potent against WT and VatA *S. aureus* when compared to flopristin (**4**). Furthermore, **47** had measurable activity (32 μg/mL) against ABC-F expressing *E. faecalis*[11,38] and *E. coli* (16 μg/mL), species that are highly resistant to streptogramins. These results support the hypothesis that modifications to C3 and C4 of the group A streptogramin scaffold can overcome resistance caused by Vat proteins while improving antimicrobial activity.

Modifications that improve the activity of the group A component may not be compatible with the B component[7]. For example, C4 extensions into the NPET may clash with the B component. Encouragingly, the combination of C3-modified **46** and even C4-modified **47** with **VS1** resulted in improved activity in many strains. In many cases, growth was completely inhibited even at the lowest concentration tested (Figure 2a). In *E. faecalis*, significant improvements in MIC were observed for **46**/**VS1** (>64, 2 μg/mL → 0.5 μg/mL) and **47**/**VS1** (32, 2 μg/mL → 0.25 μg/mL). In most strains, **47**/**VS1** was significantly more potent than linezolid and daptomycin, two antibiotics that are used to treat multidrug-resistant Gram-positive bacterial infections (see Extended Data Figure 3). These results showcase the utility of synergistic streptogramin combinations and demonstrate that group A streptogramin analogs can facilitate improved activity of the combination.

We tested **47** against an expanded panel of clinical isolates of *S. aureus* that harbor *vat* genes. *Vat* genes are often accompanied by *vga* genes, which encode ABC-class proteins that also confer resistance to group A streptogramins (Figure 2b).[13,14] Notably, strains in this panel also contained resistance genes to several other classes of antibiotics, such as β-lactams, tetracyclines, and aminoglycosides (details can be found in the CRBIP catalogue)[39]. As expected, **VM2** did not effectively inhibit the growth of these streptogramin-resistant strains. Flopristin (**4**) exhibited good to moderate activity (2–16 μg/mL), and **47** showed excellent to moderate activity (0.5–16 μg/mL). These data demonstrate that the fully synthetic, C4-modified streptogramin **47** is effective at inhibiting the growth of multidrug-resistant clinical isolates with group A streptogramin resistance genes, often with greater effectiveness than the clinical candidate flopristin (**4**).

Given the promising *in vitro* activity of **47** against streptogramin-resistant strains, we next tested its efficacy in a murine thigh model of infection using *S. aureus* CIP 111304 (strain 2), a strain that exhibits a high level of group A streptogramin resistance (Figure 2c). At 10 mg/kg, compound **47** showed a ~10-fold reduction in bacterial load compared to the 24-h infection control ($p = 0.001$, Extended Data Table 3), which was similar to high-dose flopristin (**4**) (200 mg/kg). At 200 mg/kg, **47** demonstrated a ~100-fold reduction in bacterial load compared to 24-h infection control ($p = 0.001$). It is especially notable that compound **47** demonstrates significant potency in this demanding model of infection, even in the absence of a synergistic group B streptogramin partner. Further pharmacokinetic studies are needed to better understand the observed differences in potency *in vivo* between **4** and **47**.

Mechanisms of action and resistance

In agreement with their low MIC values, **4** (IC_{50} 40 +/− 10 nM) and **47** (IC_{50} 70 +/− 20 nM) inhibited translation more effectively than **VM2** (IC_{50} 500 +/− 200 nM) *in vitro* (Figure 3a). The similar IC_{50} values of **4** and **47** suggest that their MIC differences are due to factors other than improved ribosome inhibition. To quantify deactivation by VatA, we measured C14 acetylation rates using purified VatA for **4** and **47**. The ~2.5-fold reduction in K_{cat}/K_M does not linearly account for the 8- to 16-fold reduction in MIC in the plasmid-mediated VatA *S. aureus* strain (strain 2, Figure 2a-c), but it is similar to the reduction in the MICs of the clinical isolates of *S. aureus* (strains 13–19). Nonlinear correlation of MIC value to drug deactivation can result from the contribution of other factors such as cellular accumulation,

other resistance mechanisms, and efflux[40,41]. To determine the structural contributions of **47** to a low VatA acetylation rate, we obtained an X-ray co-crystal structure (Figure 3b), which reveals displacement of Leu110 by 1.5 Å compared to **VM1** in VatA (PDB: 4HUS[2]) due to steric clash with the C4 extension of **47**.

To explore the structural basis for antimicrobial activity, we characterized several analogs bound to the *E. coli* ribosome using cryo-EM (Figure 3c,d and Extended Data Figures 5 **and** 6). The PTC is highly conserved across pathogenic species of bacteria, and the *E. coli* ribosome is an appropriate model for group A streptogramin binding in both Gram-negative and Gram-positive organisms[9]. The 2.6-Å structure of analog **47** bound to the ribosome clearly reveals the position of the C4-allyl extension, which projects towards the streptogramin B binding site and makes contact with A2062, U2585, and U2586 (Extended Data Figure 5). This extension also adopts a less strained conformation when ribosome-bound than when VatA-bound (calculated −2.3 kcal/mol, Extended Data Figure 7 and Extended Data Table 2). This difference could contribute, along with protein conformational changes (Figure 3b), to the observed acetylation rate differences between **4** and **47**. In the presence of **VS1**, the extension adopts a strained conformation similar to its conformation in VatA, but is likely stabilized by hydrophobic interactions with the B component (Figure 3d).

Ligand strain may also play a role in the efficacy of **46**. Predicted low energy conformations of **46** position the arylcarbamate extension directly over the macrocycle (Extended Data Figure 7); however, the structures of **46** bound to the ribosome in the presence or absence of **VS1** (Figure 3b and Extended Data Figure 5, respectively) showed density for the extension reaching into P-site. The isoquinoline portion of the extension sits between A2602 and C2452, without making specific contacts with either. The proximity of C29 to U2585 may explain the difference in activity between the two diastereomeric series at this position (**40a-q** and **41a-q**, Figure 1c). Consistent with this idea, **41q** demonstrated poor density for the extension with multiple conformations. Interestingly, unlike **47**, the modeled position of **46** does not clash with VatA when superposed in the crystal structure (Extended Data Figure 7). A crystal structure of **46** bound to VatA revealed an extended conformation with poor side chain density and 10 kcal/mol higher calculated internal energies (Extended Data Figure 7 and Extended Data Table 2). Collectively, these results suggest that the ligands adopt distinct, slightly strained conformations when VatA-bound than when ribosome-bound.

The bacterial PTC is a privileged antibiotic binding site (Figure 3e). It is striking that the arylcarbamate side chain in **46** and the allyl side chain in **47** do not significantly overlap with other ligands and that they maintain synergy with **VS1**. The position of the arylcarbamate side chain in **46** extends into the P-site (Figure 3f). By overlaying the 5-terminal bases of P-site bound tRNA into the structure with **46** and **VS1** bound to the catalytic center (PDB ID: 1VY4[42]), we discovered that the isoquinoline group in **46** overlaps substantially with the terminal adenosine that is conserved in all tRNAs. Only the non-selective inhibitor blasticidin, which inhibits both eukaryotic and prokaryotic ribosomes, binds this deeply into the P-site by mimicking the cytosines in the CCA tail[33]. The 23-membered macrocyclic core of the group A streptogramins will likely provide a basis for selectivity for prokaryotic ribosomes which has not been achieved by tRNA mimics such as blasticidin. Further C3 side chain optimization, guided by cryo-EM characterization, may

provide a new avenue into extremely potent, selective inhibitors of bacterial protein synthesis. This work highlights how cryo-EM is contributing to the elucidation of structure-activity relationships[43,44].

Conclusion

By combining modular chemical synthesis, antibacterial evaluation, *in vitro* analysis, and high-resolution cryo-electron microscopy, we have developed a pipeline for the synthesis and optimization of group A streptogramin antibiotics. Our approach enabled the preparation of novel analogs by means of building block variation and late-stage diversification, providing valuable structure-activity relationships for the class. Modifications at two previously unexplored positions on the scaffold afforded the first group A streptogramins to overcome resistance caused by virginiamycin acetyltransferase enzymes. These C3- and C4-modified analogs can serve as templates for optimization of both group A streptogramins and other PTC-binding antibiotics, potentially leading to candidates that overcome resistance caused by binding site modifications such as methylation of A2503 by Cfr methyltransferase. An analogy can be drawn to ketolides, such as telithromycin and solithromycin, which possess biaryl side chains that enhance activity against ribosomes modified by erythromycin methyltransferases (erm resistance) at residue A2058 in the NPET[45]. Although emergence of other resistance mechanisms is inevitable, this approach may permit chemical adaptations to extend the clinical longevity of the streptogramin class.

Methods

Minimum Inhibitory Concentration (MIC) testing

Compounds were evaluated by Micromyx LLC (Figure 2a and Extended Data Figures 3 **and** 4) and at the Collection of Institut Pasteur (Figure 2b) for Minimum Inhibitory Concentration (MIC) activity against a variety of pathogenic bacteria, using the broth microdilution method, as recommended by the Clinical and Laboratory Standards Institute (CLSI). Pre-weighed vials of the test agents were stored at −20°C until testing. On the day of the assay, the compounds were dissolved in 100% DMSO (Sigma 472301, Lot No. SHBH5551V) to a stock concentration of 6,464 μg/mL. The concentration range tested for each of the compounds was 64–0.06 μg/mL, and each compound was tested in triplicate. Levofloxacin was used as the quality control agent. For more details on test organisms, media, and methods, see the Supporting Information.

Animal study

The animal study was conducted at the University of North Texas Health Science Center following UNTHSC approved (IACUC) protocol IACUC-2017–049, which has been adapted from comparable literature methods. Test articles were supplied by the Seiple Laboratory in a randomized and blinded fashion.

Animals—Female 5–6 week-old CD-1 mice (18–22 g) were used in the studies. The mice were housed in groups of five (5) with free access to food and water during the study. Mice

were obtained from Envigo Laboratories. Animals were cared for and housed in accordance with the *Guide for Care and Use of Laboratory Animals* (National Academy Press, Washington DC, 2011). Ambient temperature was kept at 20–26°C and humidity was kept between 30% and 70%. Mice were kept on a 12:12 cycle and housed according to NIH guidelines.

Pretreatment—Mice were treated with 150 mg/kg and 100 mg/kg cyclophosphamide (Cytoxan) by the intraperitoneal (IP) route on Day −4 and Day −1.

Infection—Inoculum was prepared in Trypticase Soy Broth (TSB) from an overnight streak plate to ~10^6 CFU/mL based on previous experimental growth curve results. Animals were infected by the intramuscular (IM) route with 0.1 mL of this adjusted inoculum.

Virulence—Micromyx provided the bacterial strain, *S. aureus* VatA strain (MMX-10227, CIP 111304), including detailed data on source, purity, *in vitro* growth characterization, and antibiotic susceptibility. Mice were made neutropenic by cyclophosphamide treatment prior to infection using standard methods. Bacterial (CFU) burden was evaluated for each group at 2 hours post infection and at 24 hours post infection using standard methods involving tissue thigh homogenization followed by dilution plating to permit accurate colony counts. Mice were inoculated with 5.75 $\log_{10}$ CFU of *S. aureus* MMX-10227 (with the inoculum prepared from fresh plates with 10 μg/mL virginiamycin) and thigh samples taken at 2 and 24 hours post-infection. Plate counts performed on Mueller-Hinton Agar (MHA) + 10 μg/mL virginiamycin, Brain Heart Infusion Agar (BHI) + 0.5% charcoal, and mannitol salts agar were comparable with mean bacterial thigh titers of 6.74–6.78 $\log_{10}$ CFU at 2 hours and 8.20–8.61 $\log_{10}$ CFU at 24 hours.

Tolerance—Test articles and a vehicle dose group were administered subcutaneously in a volume of 0.5 mL. The formulation selected for use was 10% DMSO in 25% hydroxypropyl-β-cyclodextrin (hpbCD). Animals were administered a single subcutaneous dose of each test article at 50, 100, and 200 mg/kg. For each of the dose groups in the maximum tolerated dose (MTD) determination study, three (3) animals were used for each dose level. The use of three animals is sufficient for the determination of the MTD and this group size and proceeding in an ascending stepwise manner will allow for the use of as few animals as possible. Survival and general observations (breathing, mobility, reactions) as to the tolerability of the administered dose immediately following and for a period of time after each dose were recorded. Test articles were well tolerated over the dose range of 50, 100, and 200 mg/kg administered subcutaneously. There were no immediate adverse effects observed, and all animals appeared alert and responsive following observations at 0.5, 2, 14, and 24 hours after dosing.

Efficacy study—All dosing was subcutaneous starting at 2 hours post-infection. Test articles were administered as a single dose to mice at 10, 20, 50, 100, and 200 mg/kg. For each of the dose groups, five (5) animals were used at each dose level. The dosing samples were prepared fresh. Bacterial CFU/thigh at 2 hours (control) and 24 hours post-infection were determined. Animals were euthanized by CO_2 inhalation, skin reflected and thighs aseptically removed, placed in 2 mL cold sterile PBS, homogenized using a Polytron tissue

homogenizer, serially diluted and plated on Mueller-Hinton Agar + 10 μg/mL virginiamycin (MHA+V).

In vitro translation assay 10-μM screen

The ability of group A streptogramin analogs to inhibit the 70S *E. coli* ribosome was first screened using the PURExpress® *In Vitro* Protein Synthesis Kit (E6800, NEB), murine RNAse inhibitor (M0314, NEB), and 6.66 ng/μl of template DNA encoding the fluorescent protein mEGFP (gifted by the Cate lab). The volume of the reaction mixture was scaled down 5-fold from the NEB protocol for a final reaction volume of 5 μL. Analogs were screened at a final concentration of 10 μM in 10% DMSO. Translation reactions were carried out in triplicate at 37°C for 1 hour, then transferred to a 0°C metal block. To assist in the transfer of reactions to 96-well half-area Non-Binding Surface (NBS) microplates (Corning 3993) for final measurements, the reaction volume was increased to 50 μL by adding buffer (20 mM Tris-HCl pH 7.5, 60 mM NH_4Cl, 6 mM $MgCl_2$, 0.5 mM EDTA). Using a Cytation 5 plate reader (BioTek), translated mEGFP was excited at 485 nm; its emission was recorded at 535 nm. For comparison of analog activities across multiple initial screens, fluorescence readouts were normalized to the blank. Data were analyzed using Excel.

In vitro translation assay for IC_{50} determination

IC_{50} values of group A streptogramin analogs were determined using the PURExpress® Δ Ribosome Kit (E3313, NEB) for *in vitro* protein synthesis, 70S *E. coli* ribosomes (P0763S, NEB), murine RNAse inhibitor (M0314, NEB), and 6.66 ng/μl of template DNA encoding the fluorescent protein mEGFP (gifted by the Cate lab). This kit was specifically used to achieve a final ribosome concentration of 24 nM. The volume of the reaction mixture was scaled down 5-fold from the NEB protocol for a final reaction volume of 5 μL. Analogs were tested in a range from 0 to 36 μM in 10% DMSO (final concentration). Translation reactions were carried out in triplicate in a 37°C water bath for 4 hours, then transferred to a 0°C metal block. To assist in the transfer of reactions to 96-well half-area NBS microplates (Corning 3993) for final measurements, the reaction volume was increased to 50 μL by adding buffer (20 mM Tris-HCl pH 7.5, 60 mM NH_4Cl, 6 mM $MgCl_2$, 0.5 mM EDTA). Using a Cytation 5 plate reader (BioTek), translated mEGFP was excited at 485 nm; its emission was recorded at 535 nm. Raw data were processed and visualized using Python 2.7 and Matplotlib 2.0.2; the script is available on github. The IC_{50} was interpreted by fitting the dose response curve to the following equation, where *Top* and *Bottom* are the values of the plateaus: $Y = Bottom + (Top - Bottom) / (1 + (X / IC_{50}))$.

VatA cloning, expression, and purification

This protocol was adapted from Stogios *et al.*[2] The *Staphylococcus aureus* VatA sequence from residues 7 to 219 was cloned into the pET28a plasmid with an N-terminal 6xHis-tag followed by a tobacco etch virus (TEV) protease cleavage site. The plasmid was transformed into *E. coli* BL21 cells for VatA protein expression. Bacterial cultures were grown at 37°C with shaking to an OD_{600} of ~0.6–0.8, then induced with IPTG at a final concentration of 0.5 mM. After induction, the cultures were grown at 16°C with shaking and were harvested ~20–22 hours later. Cells were resuspended into 50 mL of 50 mM HEPES pH 7.8, 10 mM

imidazole pH 7.8, 300 mM NaCl, and EDTA-free protease inhibitor (#11836170001, Roche) and then sonicated using 5 rounds of 30 second pulses with a 60 second wait period. The lysate was clarified by centrifugation at 35,000 RCF for 45 minutes at 4°C. Supernatant was passed over a 5 mL Ni-NTA column (HisTrap FF, GE Healthcare), washed with 50 mM HEPES pH 7.8, 20 mM imidazole pH 7.8, 300 mM NaCl, and eluted using a 50–500 mM imidazole pH 7.8 gradient. The protein was dialysed (10,000 MWCO) into 25 mM HEPES pH 7.8, 150 mM NaCl and simultaneously cleaved using 6xHis-tagged TEV protease[46] in a 1:10 ratio by weight for 48 hours at 4°C. The sample was passed a second time through a Ni-NTA column (HisTrap FF, GE Healthcare), where VatA was collected in the wash. For enzymology, the sample was passed over a Superdex 200 16/600 sizing column (GE Healthcare) with 25 mM HEPES pH 7.8, 150 mM NaCl and collected in the elution. For both enzymology and crystallography, purified protein was concentrated and stored at −80°C until further use.

VatA acetylation assay

Acetylation assays were performed in 96-well clear polystyrene flat-bottom NBS plates (Corning 3641) at 100 μL of 50 mM HEPES pH 7.8, 0.5 mM 5,5'-dithiobis-(2-nitrobenzoic acid) (DTNB or Ellman's Reagent), 1 mM acetyl-CoA (AcCoA), 29 nM TEV-cleaved enzyme, and 0 to 0.4875 or 0.65 μM streptogramin A analog[2,47]. Analogs were diluted from stock solutions prepared at 35 mM compound in 80% ethanol; the final amount of ethanol in the acetylation reaction was 2%. All reactions were carried out in triplicate. Immediately upon adding enzyme, the reaction plate was moved to an Epoch 2 plate reader (BioTek) and its wells read at 415 nm for absorbance of the yellow TNB, a product of the 1:1 reaction of DTNB with the free sulfhydryl of CoA. Plates were read at room temperature for approximately 8 minutes with 4 second intervals between each reading of the same well. The quantity of CoA produced as a byproduct of acetylation was determined relative to a CoA standard curve, prepared in duplicate, which contained all components of the reaction solution except analog, enzyme, and AcCoA, which itself was substituted for 0 to 0.375 mM CoA, final concentrations. Linear regions and slopes of the progress curves were determined in Excel using the best fit to a linear regression model, optimizing R^2. Using the CoA standard curve, these rates were converted to VatA activity in μmol CoA/min/mg enzyme. Kinetic information was derived by fitting the data to the following Michaelis-Menten model using a script available on github.

VatA crystallization

Purified VatA was concentrated to 60 mg/mL in dialysis buffer (25 mM HEPES pH 7.8, 150 mM NaCl), mixed to a final 2:1 molar ratio (protein:compound) with 10 mM streptogramin analog in 100% DMSO, and crystallized at room temperature using the hanging drop method with a reservoir volume of 96 μL. After mixing, the samples were filtered through a 0.22-μ filter. For the VatA-**46** co-crystal structure, 100 nL of mixed sample were combined with 100 nL of 1 M LiCl, 0.1 M BICINE pH 9, and 10% w/v PEG 6K from JCSG Core II (Qiagen) using mosquito LCP (SPT Labtech). For the VatA-**47** co-crystal structure, 100 nL of mixed sample were combined with 100 nL of 0.2 M $(NH_4)_2SO_4$, 0.1 M phosphate-citrate pH 4.2, 20% v/v PEG 300, and 10% glycerol from JCSG Core II (Qiagen) using mosquito

LCP (SPT Labtech). Both crystals were cryoprotected by a brief transfer into a 2 μL mixture of 75% reservoir solution and 25% glycerol.

X-ray diffraction data collection, processing, and model building

For both crystal structures, the diffraction data was collected at the Advanced Light Source (ALS, Berkeley, CA), beamline 8.3.1, at 92 K with a wavelength of 1.11583 Å using a DECTRIS PILATUS3 6M detector. Data were processed using Xia2 (v0.6.354)[48], which used XDS (v20200131)[49] for indexing and integration and XSCALE[49] for merging. The resolution cutoff was selected automatically, using the default criteria in Xia2. Model construction was carried out using the PHENIX (v1.17.1) suite and Coot (v0.8.9.2) as follows. Structures were solved by molecular replacement using the 4HUR[2] VatA trimer and *phenix.phaser*[50]. Refinement was performed using *phenix.refine* with manual model building in Coot[51]. B-factors were refined individually for the VatA-**47** structure and as single residue groups for VatA-**46**. NCS constraints were applied in the refinement of both structures based on density and consisted of three groups: chains A + E, chains B + F, and chains C + D for VatA-**46**. The NCS constraints for VatA-**47** consisted of: chains A + F, chains B + E, and chains C + D. TLS groups were used based on those used by Stogios *et al.* for refinement of VatA[2]. Both VatA-**46** and VatA-**47** were refined with the OPLS3e/VSGB2.1 force field from Schrödinger as described below but using *phenix.refine* to obtain low energy conformations for the ligands. Data collection and refinement statistics are reported in Extended Data Table 2. To obtain low energy conformations of **VM1** in VatA and the *E. coli* ribosome, respectfully from 4HUS[2] and 4U25[9], the models were refined once using *phenix.refine* and the **VM1** ligand refined with the OPLS3e/VSGB2.1 force field. Ligand energies were then evaluated by Prime with OPLS3e/VSGB2.1 (Extended Data Table 2).

CryoEM sample preparation

For CryoEM analysis, purified 50S ribosomes from *E. coli* strain MRE600[52] were prepared in 50 mM HEPES pH 7.5, 150 mM KOAc, 6 mM MgAc, and 7 mM fresh β-mercaptoethanol (BME). Inhibitor was added, mixed gently, and incubated on ice for 1 hour. The final concentration of ribosomes was 100 nM; the final concentration of each inhibitor was 60 μM. For samples prepared with two inhibitors, both were added in a 1:1 ratio. For each grid (Quantifoil holey carbon grids, C2-C14nCu30–01 or N1-C14nCu40–01, Quantifoil Micro Tools Gmbh), 3.5 μL of sample was deposited onto a freshly glow-discharged (EMS-100 Glow Discharge System, Electron Microscopy Sciences, 30 seconds at 15 mA) grid and incubated for 30 seconds at 25°C and 100% humidity. Grids were vitrified by plunge-freezing into liquid ethane[53] using a FEI Vitrobot Mark IV (ThermoFisher). To achieve optimal ice quality for collection, liquid was blotted from the grid using Whatman #1 filter paper and multiple grids for each sample were frozen with a range of different blotting times. Grids were screened using a FEI Talos Arctica electron microscope (ThermoFisher, operating at 200 kV, located at UCSF) to check ice quality and identify the optimum grids for data collection.

CryoEM data collection

All data sets were collected on FEI Titan Krios electron microscopes (ThermoFisher, operating at 300 kV, located at UCSF or NCCAT), with the exception of **40q**, which was collected on a FEI Talos Arctica electron microscope (ThermoFisher, operating at 200 kV, located at UCSF). Automated data collection at UCSF was facilitated by SerialEM (v3.6)[54]; collection at NCCAT was via Leginon (v3.4)[55]. The 50S with **47**/**VS1** bound dataset was collected on a K3 (Gatan) Direct Electron Detector (DED) with a Gatan Imaging Filter (Gatan, 20 eV slit) using a nine-shot beam-image shift approach with coma compensation[56]. The 50S with **47** bound and the 50S with **46**/**VS1** bound datasets were collected using a four-shot beam-image shift approach with coma compensation on a K2 Summit DED (Gatan). All other datasets were collected on-axis using a K2 Summit DED (Gatan). Pixel sizes, number of images in dose-fractionated micrographs, dose rates, and defocus ranges varied slightly and are reported in Extended Data Table 1. All image stacks were collected in super-resolution mode.

CryoEM image and data processing

Super-resolution image stacks were binned by a factor of 2, corrected for beam-induced motion, and dose-weighted using MotionCor2 (v1.2.1)[57]. All Coulomb potential density maps were reconstructed in cisTEM (1.0.0-beta)[58] using dose-weighted micrographs. Initial CTF parameters were determined using CTFFIND4, included as part of the cisTEM package, with the resolution range between 30 and 4 Å included in the fitting. Bad micrographs (crystalline ice, poor CTF fits) were excluded from processing through visual inspection. Particles were picked in cisTEM by matching to a soft-edged disk template with a maximum particle radius of 110 Å and a characteristic particle radius of 90 Å. The number of particles picked from all micrographs and from good micrographs are found in Extended Data Table 1. CisTEM refinement packages were made using a particle molecular weight of 1800 kDa. Particles were 2D-classified into 50 classes with a mask radius of 150 Å. Classes containing the 50S ribosome were carried forward into single-class auto refinement with an outer mask radius of 125 Å and a default starting resolution of 20 Å. A filtered volume was used to make a binary mask; the volume eraser tool from UCSF Chimera (v1.12)[59] was used to exclude the mobile L1 stalk from the mask. This mask was used in single-class manual refinement with a final high-resolution limit of either 3.50 or 3.00 Å (see Extended Data Table 1). Unsharpened maps were used in model refinement and for all figures.

CryoEM model building and refinement with OPLS3e

We used UCSF Chimera (v1.12) to rigid body align a high resolution X-ray structure of the *E. coli* ribosome (PDB ID: 4YBB[60]) into our maps. Principle versions of the PHENIX suite used for CryoEM model building were 1.14, dev-3406, 1.16, and 1.17. Initially, the ligand restraints files (CIF files) were generated with *phenix.eLBOW*[61] using the analog's SMILES string and a "final geometry" reference pdb of the analog that was derived from the pose of flopristin bound to the *E. coli* ribosome (PDB ID: 4U20[9]). These ligands were superimposed into 4YBB based on the binding pose of flopristin in 4U20, and manual edits to the surrounding structure were performed in Coot (v0.8.9.2).

After constructing these initial models, structures were refined using *phenix.real_space_refine* with the default protocol, initially with CIF restraints files from *phenix.eLBOW*. These resulted, however, in non-physical high energy conformations of the ligands (Extended Data Figure 1 and Extended Data Table 1). To improve the models of the ligands, we used a new version of *phenix.real_space_refine* interfaced with the OPLS3e/VSGB2.1 force field, a high quality force field for ligands[62]. This approach allows obtaining physics-based energies and gradients for either the whole or part of the structure without resorting to accurate manual CIF restraint generation. Standard PHENIX restraints were used for the macromolecule, while the ligand was governed by the OPLS3e/VSGB2.1 force field. Precisely, the unliganded complex and ligand were individually prepped using *phenix.ready_set* and *prepwizard*, respectively, and subsequently recombined. The recombined complex served as input for refinement using the additional Schrödinger-dependent options *use_schrodinger=True maestro_file=ligand.mae schrodinger.selection="resname LIG"*, where *ligand.mae* describes the ligand structure in Maestro format and LIG is the residue 3-letter code, and otherwise default parameters. For models with two ligands, namely **46**/**VS1** and **47**/**VS1**, **VS1** was prepared in the same way as the ligand described above. All refinement for **46**/**VS1** and **47**/**VS1** was carried out using PHENIX-OPLS3e/VSGB2.1. Coordinates for **VS1** and the companion ligand were merged into one instance in Maestro and exported to one .mae file. Both ligands were included in the Schrödinger selection for OPLS3e refinement.

The PHENIX-OPLS3e/VSGB2.1 interface works as follows: the PHENIX refinement engine spawns an external process serving as an energy server, initialized with the ligand structure present in the provided *maestro_file* option. When the refinement engine requests energies and gradients, the ligand's internal coordinates are written to file and read in by the external server. After updating ligand coordinates on the server side, the energy and gradients are calculated and exchanged with the refinement engine. The refinement engine on its side updates the ligand energy and gradients contribution in its energy function using a default weight factor of 10 for the OPLS3e/VSGB2.1 energies. Refinement with the OPLS3e/VSGB2.1 force field reduced the energy for all ligands compared to the conformations refined using CIF based restraints calculated by *phenix.eLBOW* (Extended Data Table 1).

For all CryoEM figures, the full, unsharpened density maps and full pdb models were boxed using *phenix.map_box* with a selection radius of 20 Å around the ligand(s). Boxed map and model were loaded into PyMol (incentive v2.2.3) with *set normalize_ccp4_maps, off*. Maps were contoured at 4σ for tight density (dark blue) and 1σ for loose density (light gray), both centered around the ligand with a carve of 1.8.

QM calculations

Calculations were based on the scaffold of flopristin (**4**) from the crystal structure bound to the ribosome[9]. Compound **46** was constructed using the LigPrep tool of Maestro (v2019–4, Schrödinger Inc.). First, the macrocycle conformation sampling method[63] was validated by comparison to the low energy pose as that of the co-crystal structure of flopristin (**4**). By using the thorough sampling intensity strategy, 1000 conformations of **46** were obtained, and

the lowest prime energy pose with the RMSD <2 Å (scaffold atoms of **4** as reference atoms) was regarded as the preferred conformation. Finally, the C3 side chain of this preferred conformation was further optimized using Jaguar software[64] using the B3LYP/6–31G* basis set by imposing the constraints on the scaffold atoms.

Statistical analyses

Statistical evaluation of data was carried out in Microsoft Excel as follows: Murine thigh infection model data (24-hour control, **4**, **47**) were analyzed using a one-way ANOVA followed by a post hoc Tukey's test. MIC data (**4**, **47**) in strain 2 (CIP 111304) were evaluated by a Mann-Whitney U Test. Kinetics data (**4**, **47**) were analyzed using a two-tailed unpaired t-test and a Cohen's d. All values are reported in Extended Data Table 3.

Extended Data

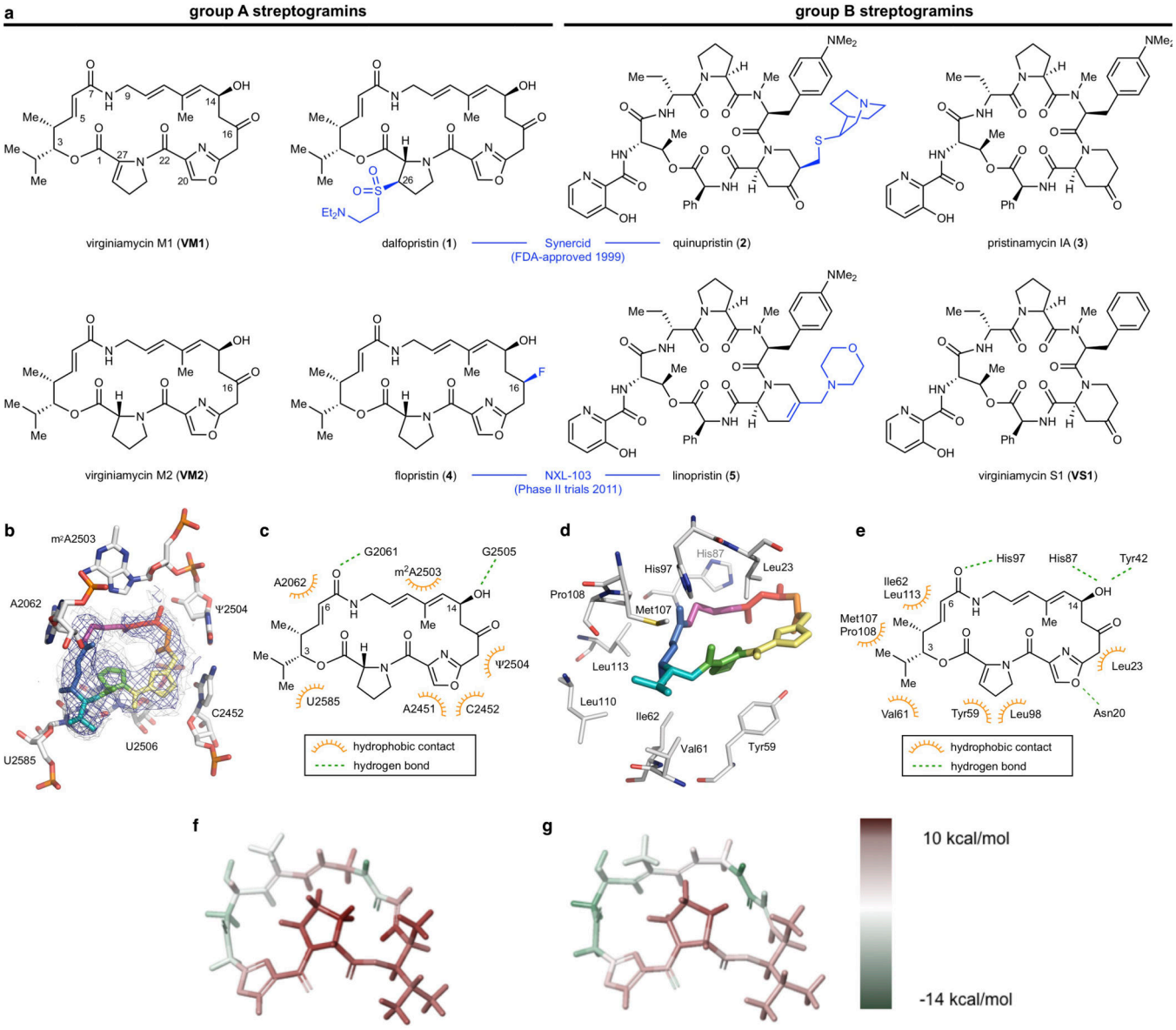

Extended Data Figure 1 |. Natural and semisynthetic streptogramins and their molecular mechanisms of action and resistance.

a, Selected natural and semisynthetic streptogramin analogs. Modifications installed by semisynthesis are highlighted in blue. **b**, 2.5-Å cryo-EM structure of **VM2** bound to the 50S subunit of the *E. coli* ribosome. Coulomb potential density is contoured in dark blue at 4.0σ and light gray at 1.0σ. Atom coloring of **VM2** mirrors the building blocks used in its synthesis (see Figure 2). **c**, Binding interactions between **VM2** and residues in the ribosomal binding site. **d**, X-ray crystal structure **VM1** bound to the resistance protein VatA (PDB ID: 4HUS). **e**, Binding interactions between **VM1** and VatA, highlighting the extensive hydrophobic interactions at C3-C6. Acetylation occurs at the C14 alcohol. **f**,**g**, Conformational energy of VM2 showing contributions on a per atom basis when refined

with standard CIF-based restraints generated by *phenix.eLBOW* (**f**) and when refined with OPLS3e/VSGB2.1 force field (**g**). Color indicates low strain (green, −14 kcal/mol) up to high strain (red, 10 kcal/mol), with total conformational energy of 39.5 kcal/mol (**f**) and −88.3 (**g**). Hydrogens were added and optimized with fixed heavy atoms for the CIF-based refined conformation using *prepwizard*; the PHENIX-OPLS3e/VSGB2.1 refined conformation was taken as is. Energies were calculated using Prime and per atom contribution visualized using Maestro's Prime Energy Visualization.

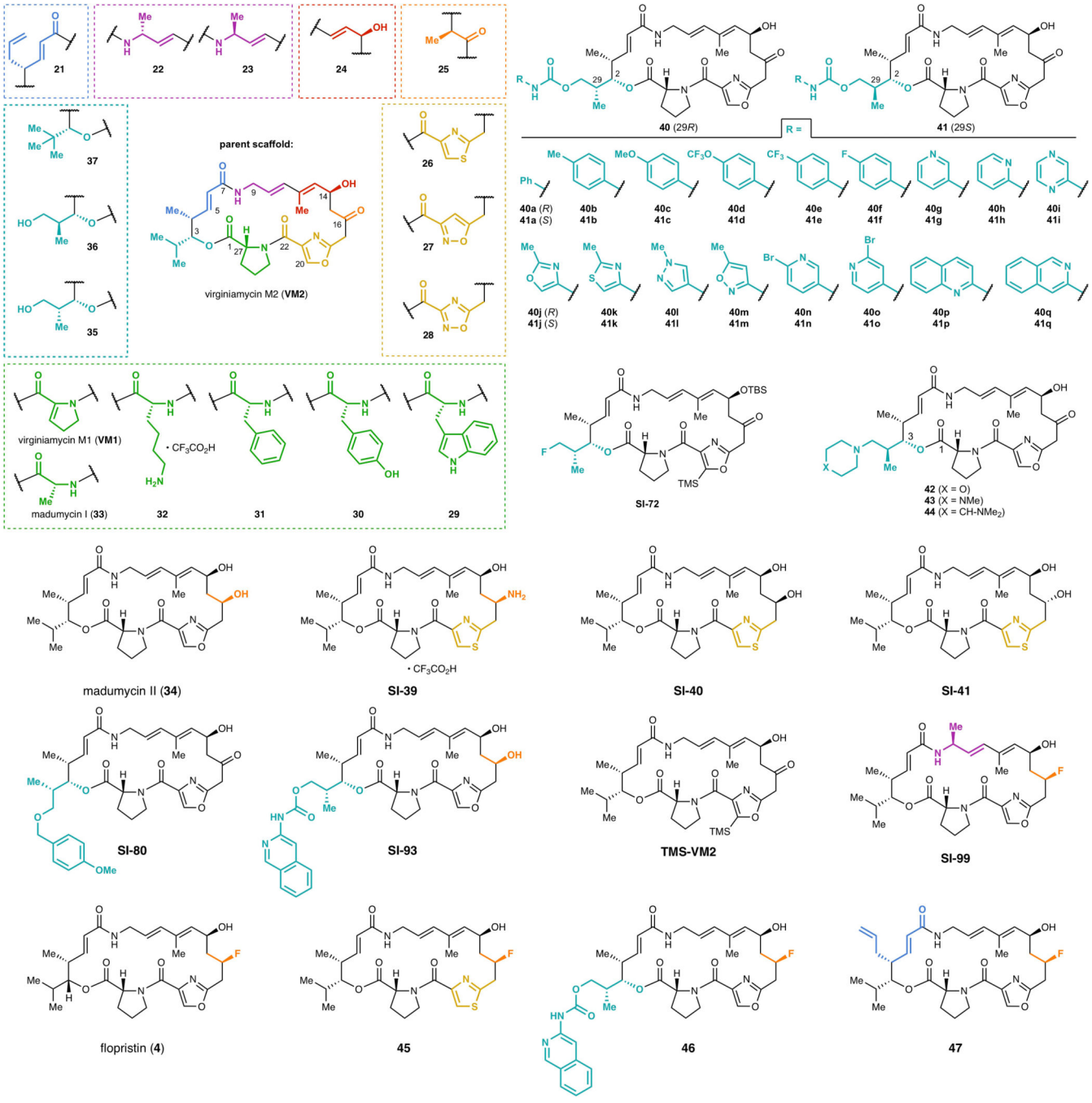

Extended Data Figure 2 - List of streptogramins tested for inhibitory activity

Fully synthetic group A streptogramins tested for inhibitory activity against 21 strains of bacteria (see Extended Data Figures 3 **and** 4).

Minimal Inhibitory Concentration (MIC) Values (μg/mL)

Compound ID	SA Barcode	*E. faecalis* CLSI QC; *In vivo* strain MMX 0101; ATCC 29212	*E. faecium* ATCC isolate; VSE MMX 709; ATCC 35667	*E. faecium* VRE; vanA MMX 0752	*S. aureus* CLSI QC MMX 100; ATCC 29213	*S. aureus* VatA streptogramin acetyltransferase-mediated resistance CIP 111304; MMX 10227	*S. aureus* MRSA MMX 2001; ATCC 33591	*S. aureus* MLSb EmA resistance; inducible MMX 2321; BAA-977	*S. aureus* MLSb EmA resistance; constitutive MMX 3035	*S. aureus* Linezolid-resistant; cfr MMX 3067	*S. pneumoniae* PSSP; CLSI QC MMX 1195; ATCC 49619
VM2	SA0106120	>64	4	8	16	>64	16	32	8	>64	8
VM1	SA0106145	64	2	8	4	32	2	8	2	>64	8
madumycin I (33)	SA0106141	32	2	4	8	64	8	8	4	64	4
madumycin II (34)	SA0106143	>64	0.5	8	8	>64	8	16	8	>64	4
21	SA0601037	64	2	4	4	16	4	4	2	>64	8
22	SA0112091	>64	>64	>64	>64	>64	>64	>64	>64	>64	64
23	SA0112090	64	>64	>64	>64	>64	>64	>64	>64	>64	64
24	SA0110239	>64	>64	>64	>64	>64	>64	>64	>64	>64	64
25	SA0112078	64	64	>64	64	64	64	>64	64	>64	64
26	SA0110141	>64	4	8	16	64	16	16	8	>64	8
27	SA05101042	>64	>64	>64	>64	>64	>64	>64	>64	>64	>64
28	SA05101054	>64	>64	>64	>64	>64	>64	>64	>64	>64	64
29	SA0202089	>64	32	32	32	64	32	32	32	>64	32
30	SA0202097	>64	>64	>64	>64	>64	>64	>64	>64	>64	64
31	SA0202061	32	32	64	64	64	64	64	64	>64	16
32	SA0202094	>64	>64	>64	>64	>64	>64	>64	>64	>64	>64
35	SA0110170	>64	>64	>64	>64	>64	>64	>64	>64	>64	64
36	SA0110026	>64	64	>64	>64	>64	>64	>64	>64	>64	64
37	SA0306004	>64	32	>64	32	>64	64	64	32	>64	64
42	SA0110161	>64	>64	>64	>64	>64	>64	>64	>64	>64	>64
43	SA0110241	>64	>64	>64	>64	>64	>64	>64	>64	>64	>64
44	SA0110252	>64	>64	>64	>64	>64	>64	>64	>64	>64	>64
40a	SA0110196	>64	16	64	32	>64	32	64	16	>64	32
40b	SA0110184	>64	16	16	16	>64	16	32	16	>64	32
40c	SA0110185	>64	16	32	32	>64	16	32	16	>64	32
40d	SA0110195	>64	8	>64	16	>64	16	16	8	>64	>64
40e	SA0110193	>64	8	>64	8	16	8	16	8	>64	>64
40f	SA0110180	>64	16	16	32	>64	16	32	16	>64	32
40g	SA0110205	>64	32	64	>64	>64	>64	>64	>64	>64	32
40h	SA0110222	>64	32	64	>64	>64	>64	>64	64	>64	32
40i	SA0110215	>64	64	>64	>64	>64	>64	>64	>64	>64	64
40j	SA0110210	>64	64	64	>64	>64	>64	>64	>64	>64	64
40k	SA0110214	>64	32	64	64	>64	64	>64	64	>64	32
40l	SA0110218	>64	>64	>64	>64	>64	>64	>64	>64	>64	>64
40m	SA0110225	>64	32	64	>64	>64	64	>64	64	>64	32
40n	SA0110209	>64	16	>64	16	>64	16	>64	16	>64	16
40o	SA0110206	>64	8	16	16	>64	16	32	16	>64	8
40p	SA0110223	>64	4	16	8	32	8	16	4	>64	32
40q	SA0110224	>64	4	8	4	16	4	8	4	>64	16
41a	SA0110043	>64	16	64	32	>64	32	64	32	>64	16
41b	SA0110037	>64	16	64	32	>64	32	64	16	>64	16
41c	SA0110040	>64	16	64	32	>64	32	64	16	>64	16
41d	SA0110041	>64	8	>64	>64	>64	>64	>64	32	>64	>64
41e	SA0110044	>64	16	>64	>64	>64	>64	>64	32	>64	>64
41e	SA0111044	>64	>64	>64	>64	>64	>64	>64	>64	>64	>64
41f	SA0110036	>64	8	32	32	>64	32	>64	16	>64	16
41g	SA0110067	>64	32	>64	>64	>64	>64	>64	64	>64	32
41h	SA0110120	>64	32	64	64	>64	64	>64	32	>64	16
41i	SA0110101	>64	64	>64	>64	>64	>64	>64	>64	>64	32
41j	SA0110095	>64	32	>64	>64	>64	>64	>64	64	>64	16
41k	SA0110098	>64	16	64	64	>64	32	64	32	>64	16
41l	SA0110113	>64	64	>64	>64	>64	>64	>64	>64	>64	8
41m	SA0110115	>64	32	>64	>64	>64	>64	>64	64	>64	16
41n	SA0110082	>64	32	>64	>64	>64	>64	>64	32	>64	8
41o	SA0110081	>64	32	>64	>64	>64	>64	>64	32	>64	32
41p	SA0110117	>64	16	32	16	>64	16	32	16	>64	4
41q	SA0110118	>64	4	16	8	>64	8	16	8	>64	2
SI-39	SA0110268	>64	64	>64	>64	>64	>64	>64	>64	>64	32
SI-40	SA0110264	>64	1	4	8	>64	16	16	8	>64	2
SI-41	SA0110266	>64	>64	>64	>64	>64	>64	>64	>64	>64	>64
SI-72	SA0110273	>64	16	64	64	>64	64	64	32	>64	16
SI-80	SA0110016	32	32	64	64	64	64	64	64	64	16
SI-93	SA0111221B	>64	8	>64	16	>64	16	32	16	>64[a]	8
SI-99	SA0112129	>64	>64	>64	>64	>64	>64	>64	>64	>64	>64
TMS-VM2	SA0110261	>64	64	>64	>64	>64	64	>64	64	>64	64
flopristin (4)	SA0110272	>64	0.5	2	0.5	8	0.5	1	0.5	>64	2
45	SA0110279	>64	0.5	1	0.5	8	0.5	1	0.5	>64	1
46	SA0111223	>64	2	2	2	1	0.5	0.5	0.25	>64	2
47	SA0112131	32	0.12	0.5	0.12	0.5	0.25	0.25	0.12	>64	1
VS1	SB0306015	2	2	64	8	16	8	4	8	8	1
VM1 + VS1	SAB0306016	1	≤0.06	0.25	0.12	16	12	0.25	1	8	0.12
flopristin (4) + VS1	SA0113191	0.5	≤0.06	≤0.06	0.12	4	0.5	0.12	0.5	16	0.12
46 + VS1	SAB0306017	0.5	≤0.06	0.12	0.25	1	0.25	0.25	0.12	4	≤0.06
47 + VS1	SAB0306018	0.25	≤0.06	≤0.06	≤0.06	1	0.5	≤0.06	0.12	4	≤0.06
linezolid	-	1-4	2	nt	0.12-1	nt	1	2	2	16	0.25-2
daptomycin	-	1-4	2	nt	1-4	nt	1	nt	nt	0.25	0.06-0.5

Extended Data Figure 3 -

Inhibitory activity against Gram-positive organisms

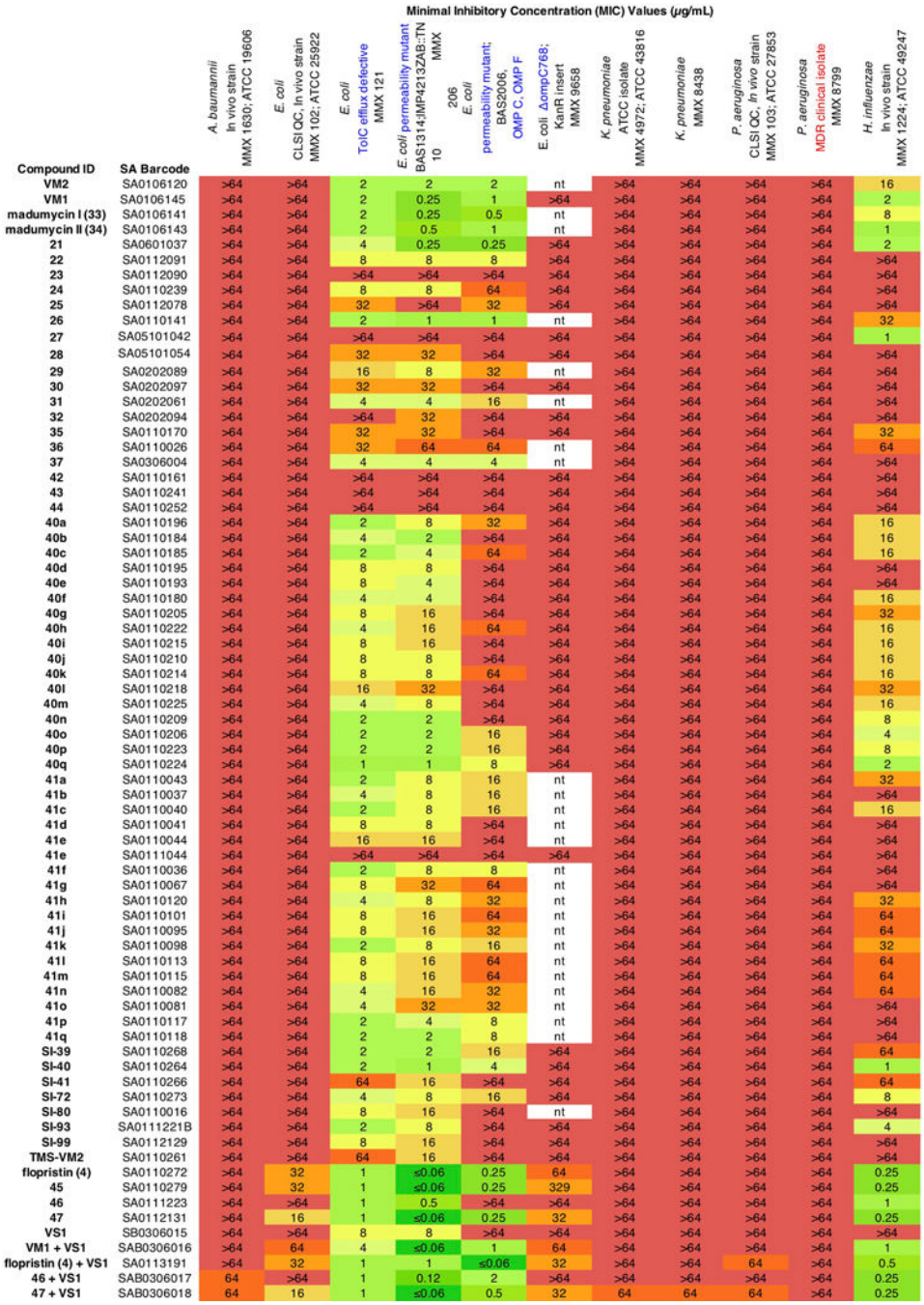

Compound ID	SA Barcode	A. baumannii In vivo strain MMX 1630; ATCC 19606	E. coli CLSI QC, In vivo strain MMX 102; ATCC 25922	E. coli TolC efflux defective MMX 121	E. coli permeability mutant BAS1314;IMP4213ZAB::TN MMX 10	E. coli permeability mutant; BAS2006, OMP C, OMP F	E. coli ΔompC768; KanR insert MMX 9658	K. pneumoniae ATCC isolate MMX 4972; ATCC 43816	K. pneumoniae MMX 8438	P. aeruginosa CLSI QC, In vivo strain MMX 103; ATCC 27853	P. aeruginosa MDR clinical isolate MMX 8799	H. influenzae In vivo strain MMX 1224; ATCC 49247
VM2	SA0106120	>64	>64	2	2	2	nt	>64	>64	>64	>64	16
VM1	SA0106145	>64	>64	2	0.25	1	>64	>64	>64	>64	>64	2
madumycin I (33)	SA0106141	>64	>64	2	0.25	0.5	nt	>64	>64	>64	>64	8
madumycin II (34)	SA0106143	>64	>64	2	0.5	1	nt	>64	>64	>64	>64	1
21	SA0601037	>64	>64	4	0.25	0.25	>64	>64	>64	>64	>64	2
22	SA0112091	>64	>64	8	8	8	>64	>64	>64	>64	>64	>64
23	SA0112090	>64	>64	>64	>64	>64	>64	>64	>64	>64	>64	>64
24	SA0110239	>64	>64	8	8	64	>64	>64	>64	>64	>64	>64
25	SA0112078	>64	>64	32	>64	32	>64	>64	>64	>64	>64	>64
26	SA0110141	>64	>64	2	1	1	nt	>64	>64	>64	>64	32
27	SA05101042	>64	>64	>64	>64	>64	>64	>64	>64	>64	>64	1
28	SA05101054	>64	>64	32	32	>64	>64	>64	>64	>64	>64	>64
29	SA0202089	>64	>64	16	8	32	nt	>64	>64	>64	>64	>64
30	SA0202097	>64	>64	32	32	>64	>64	>64	>64	>64	>64	>64
31	SA0202061	>64	>64	4	4	16	nt	>64	>64	>64	>64	>64
32	SA0202094	>64	>64	>64	32	>64	>64	>64	>64	>64	>64	>64
35	SA0110170	>64	>64	32	32	>64	>64	>64	>64	>64	>64	32
36	SA0110026	>64	>64	32	64	64	nt	>64	>64	>64	>64	64
37	SA0306004	>64	>64	4	4	4	nt	>64	>64	>64	>64	>64
42	SA0110161	>64	>64	>64	>64	>64	>64	>64	>64	>64	>64	>64
43	SA0110241	>64	>64	>64	>64	>64	>64	>64	>64	>64	>64	>64
44	SA0110252	>64	>64	>64	>64	>64	>64	>64	>64	>64	>64	>64
40a	SA0110196	>64	>64	2	8	32	>64	>64	>64	>64	>64	16
40b	SA0110184	>64	>64	4	2	>64	>64	>64	>64	>64	>64	16
40c	SA0110185	>64	>64	2	4	64	>64	>64	>64	>64	>64	16
40d	SA0110195	>64	>64	8	8	>64	>64	>64	>64	>64	>64	>64
40e	SA0110193	>64	>64	8	4	>64	>64	>64	>64	>64	>64	>64
40f	SA0110180	>64	>64	4	4	>64	>64	>64	>64	>64	>64	16
40g	SA0110205	>64	>64	8	16	>64	>64	>64	>64	>64	>64	32
40h	SA0110222	>64	>64	4	16	64	>64	>64	>64	>64	>64	16
40i	SA0110215	>64	>64	8	16	>64	>64	>64	>64	>64	>64	16
40j	SA0110210	>64	>64	8	8	>64	>64	>64	>64	>64	>64	16
40k	SA0110214	>64	>64	8	8	64	>64	>64	>64	>64	>64	16
40l	SA0110218	>64	>64	16	32	>64	>64	>64	>64	>64	>64	32
40m	SA0110225	>64	>64	4	8	>64	>64	>64	>64	>64	>64	16
40n	SA0110209	>64	>64	2	2	>64	>64	>64	>64	>64	>64	8
40o	SA0110206	>64	>64	2	2	16	>64	>64	>64	>64	>64	4
40p	SA0110223	>64	>64	2	2	16	>64	>64	>64	>64	>64	8
40q	SA0110224	>64	>64	1	1	8	>64	>64	>64	>64	>64	2
41a	SA0110043	>64	>64	2	8	16	nt	>64	>64	>64	>64	32
41b	SA0110037	>64	>64	4	8	16	nt	>64	>64	>64	>64	>64
41c	SA0110040	>64	>64	2	8	16	nt	>64	>64	>64	>64	16
41d	SA0110041	>64	>64	8	8	>64	nt	>64	>64	>64	>64	>64
41e	SA0110044	>64	>64	16	16	>64	nt	>64	>64	>64	>64	>64
41e	SA0111044	>64	>64	>64	>64	>64	>64	>64	>64	>64	>64	>64
41f	SA0110036	>64	>64	2	8	8	nt	>64	>64	>64	>64	>64
41g	SA0110067	>64	>64	8	32	64	nt	>64	>64	>64	>64	>64
41h	SA0110120	>64	>64	4	8	32	nt	>64	>64	>64	>64	32
41i	SA0110101	>64	>64	8	16	64	nt	>64	>64	>64	>64	64
41j	SA0110095	>64	>64	8	16	32	nt	>64	>64	>64	>64	64
41k	SA0110098	>64	>64	2	8	16	nt	>64	>64	>64	>64	32
41l	SA0110113	>64	>64	8	16	64	nt	>64	>64	>64	>64	64
41m	SA0110115	>64	>64	8	16	64	nt	>64	>64	>64	>64	64
41n	SA0110082	>64	>64	4	16	32	nt	>64	>64	>64	>64	64
41o	SA0110081	>64	>64	4	32	32	nt	>64	>64	>64	>64	>64
41p	SA0110117	>64	>64	2	4	8	nt	>64	>64	>64	>64	>64
41q	SA0110118	>64	>64	2	2	8	nt	>64	>64	>64	>64	>64
SI-39	SA0110268	>64	>64	2	2	16	>64	>64	>64	>64	>64	64
SI-40	SA0110264	>64	>64	2	1	4	>64	>64	>64	>64	>64	1
SI-41	SA0110266	>64	>64	64	16	>64	>64	>64	>64	>64	>64	64
SI-72	SA0110273	>64	>64	4	8	16	>64	>64	>64	>64	>64	8
SI-80	SA0110016	>64	>64	8	16	>64	nt	>64	>64	>64	>64	>64
SI-93	SA0111221B	>64	>64	2	8	>64	>64	>64	>64	>64	>64	4
SI-99	SA0112129	>64	>64	8	16	>64	>64	>64	>64	>64	>64	>64
TMS-VM2	SA0110261	>64	>64	64	16	>64	>64	>64	>64	>64	>64	>64
flopristin (4)	SA0110272	>64	32	1	≤0.06	0.25	64	>64	>64	>64	>64	0.25
45	SA0110279	>64	32	1	≤0.06	0.25	329	>64	>64	>64	>64	0.25
46	SA0111223	>64	>64	1	0.5	>64	>64	>64	>64	>64	>64	1
47	SA0112131	>64	16	1	≤0.06	0.25	32	>64	>64	>64	>64	0.25
VS1	SB0306015	>64	>64	8	8	>64	>64	>64	>64	>64	>64	>64
VM1 + VS1	SAB0306016	>64	64	4	≤0.06	1	64	>64	>64	>64	>64	1
flopristin (4) + VS1	SA0113191	>64	32	1	1	≤0.06	32	>64	>64	64	>64	0.5
46 + VS1	SAB0306017	64	>64	1	0.12	2	>64	>64	>64	>64	>64	0.25
47 + VS1	SAB0306018	64	16	1	≤0.06	0.5	32	64	64	64	>64	0.25

Extended Data Figure 4 -
Inhibitory activity against Gram-negative organisms

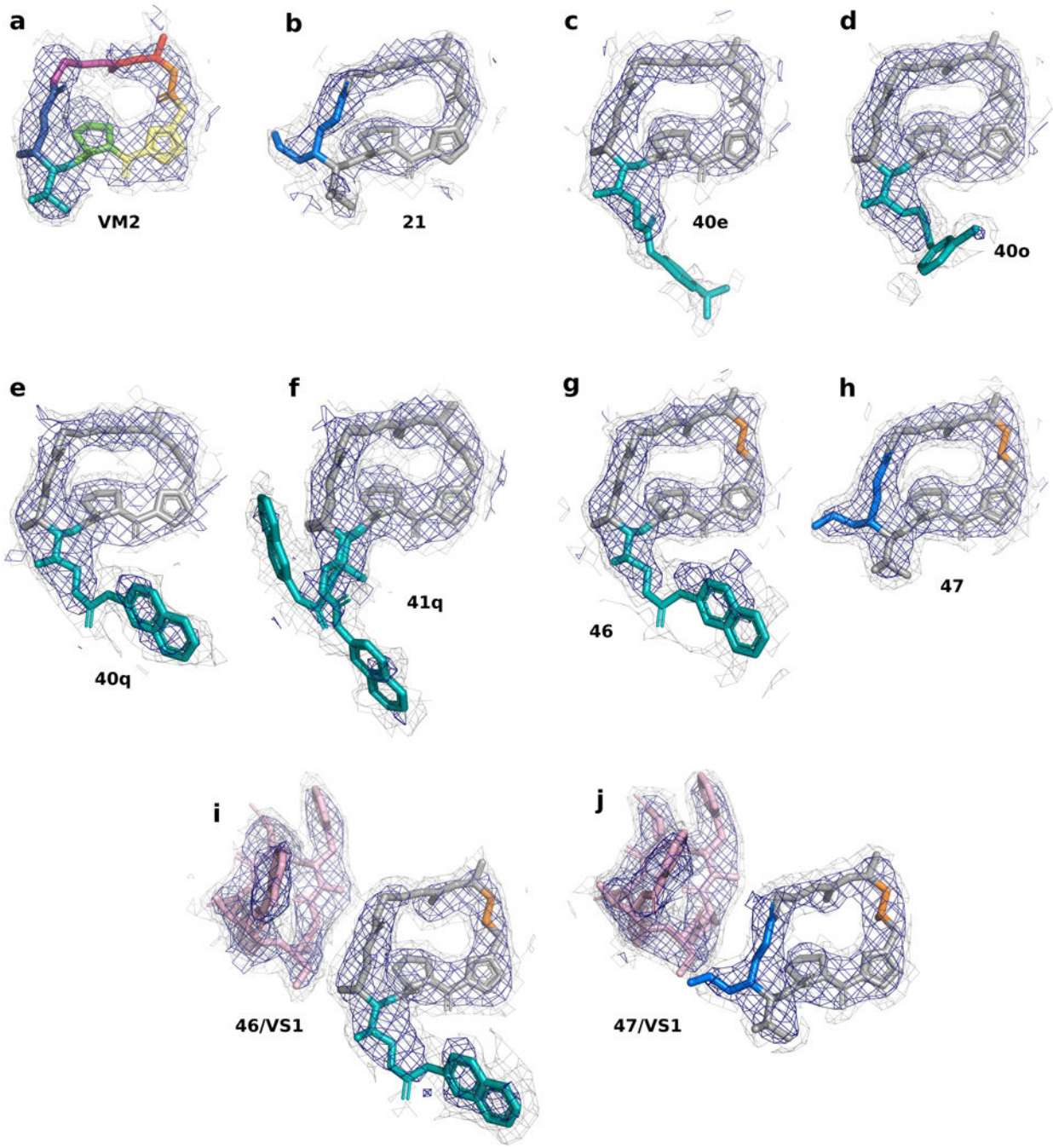

Extended Data Figure 5 - CryoEM Density for all compounds bound to the E coli ribosome

a, 2.6-Å CryoEM structure of **VM2** bound to the 50S subunit of the *E. coli* ribosome. Coulomb potential density is contoured in dark blue at 4.0σ and light gray at 1.0σ for entire figure. **b**, 2.8-Å CryoEM structure of **21** bound to the 50S subunit of the *E. coli* ribosome. **c**, 2.8-Å CryoEM structure of **40e** bound to the 50S subunit of the *E. coli* ribosome. **d**, 2.5-Å CryoEM structure of **40o** bound to the 50S subunit of the *E. coli* ribosome. **e**, 2.8-Å CryoEM structure of **40q** bound to the 50S subunit of the *E. coli* ribosome. **f**, 2.6-Å CryoEM structure of **41q** bound to the 50S subunit of the *E. coli* ribosome. **g**, 2.5-Å CryoEM structure of **46**

bound to the 50S subunit of the *E. coli* ribosome. **h**, 2.5-Å CryoEM structure of **47** bound to the 50S subunit of the *E. coli* ribosome. **i**, 2.7-Å CryoEM structure of **46**/**VS1** bound to the 50S subunit of the *E. coli* ribosome. **j**, 2.8-Å CryoEM structure of **47**/**VS1** bound to the 50S subunit of the *E. coli* ribosome.

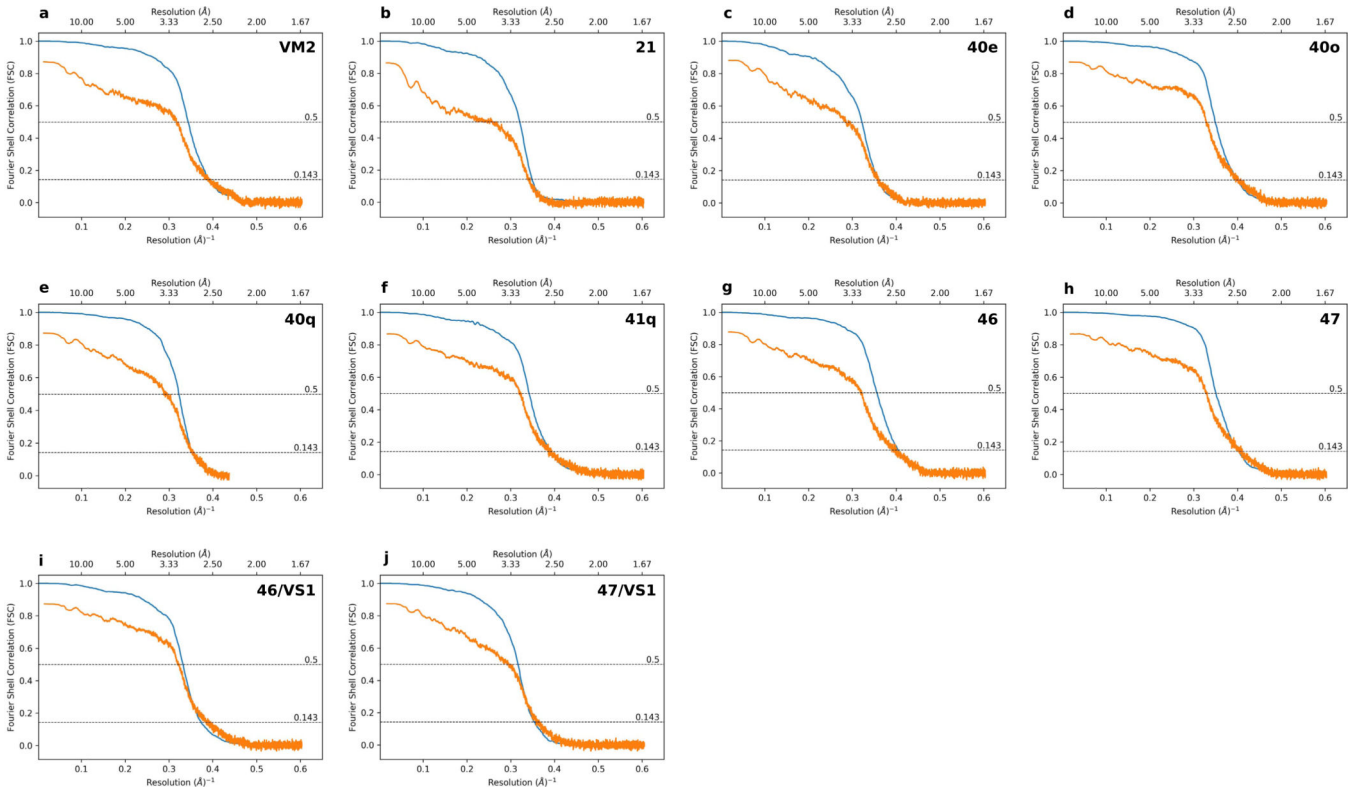

Extended Data 6 - Gold Standard and Map to Model Fourier Shell Correlation plots

a-j, The particle Fourier Shell Correlation (FSC) curves for reconstructions obtained by cisTEM using a molecular weight of 1.8 MDa are shown in blue with unmasked Map-Model FSC curves obtained from *phenix.mtriage* shown in orange. Dashed lines indicate FSC of 0.143 for estimating Gold Standard resolution and FSC of 0.5 for estimating Map-Model resolution.

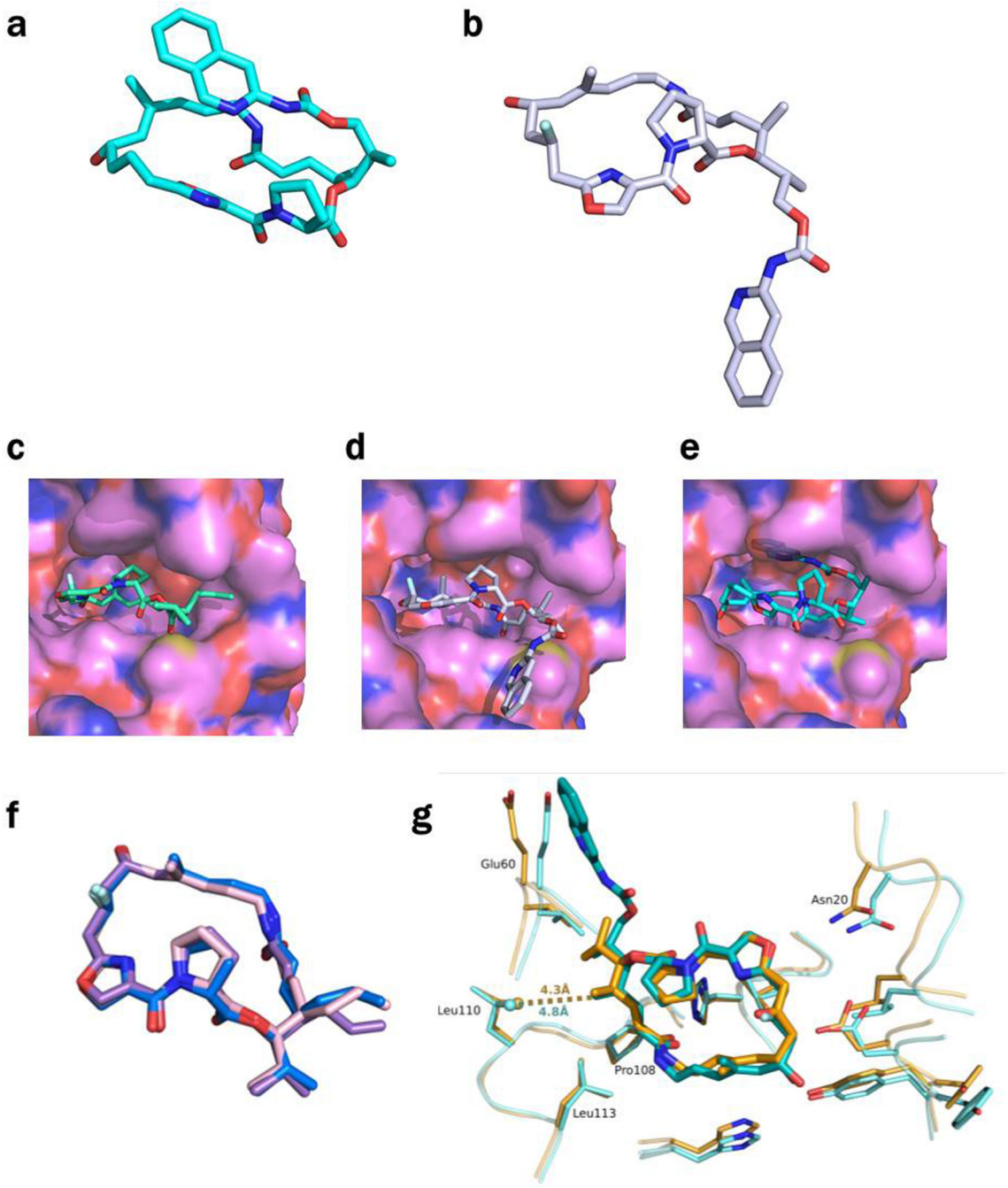

Extended Data Figure 7 - Conformations of 46 and 47 in the ribosome and in VatA

a, The conformation of **46** minimized by QM methods in low dielectric, shows how the isoquinoline side chain packs over the macrocycle. **b**, In contrast, the ribosome-bound conformations of **46** determined by CryoEM show that the side chain extends away from the macrocycle due to interactions formed in the binding site. **c**, Model of **47** in the conformation bound to the ribosome modeled into the active site of VatA (shown in surface). **d**, Model of **46** in the conformation bound to the ribosome modeled into the active site of VatA. **e,** Low energy model of **46** modeled into the active site of VatA. **f**, Overlay of VatA-

bound (marine), ribosome-bound (violet), and ribosome with **VS1**-bound (light pink) conformations of **47**. **g**, X-ray crystal structures of **VM1** bound to VatA (PDB ID: 4HUS, 2.4 Å) and **46** bound to VatA at 2.8-Å resolution.

Extended Data Table 1 - Ligand energies by different refinement schemes

Comparative table of ligand energies when ligands are refined using *phenix.eLBOW* generated restraints and the PHENIX force field versus when ligands are decoupled from the receptor environment and refined with PHENIX-OPLS3e/VSGB2.1. Energies were evaluated by Prime with OPLS3e/VSGB2.1.

Compound	Energy CIF refinement (kcal/mol)	Energy OPLS3e/VSGB2.1 (kcal/mol)	Delta (kcal/mol)
VM2	65.80	−93.28	−159.08
21	146.35	−91.09	−237.44
40e	702.53	−127.58	−829.11
40o	128.09	−136.21	−264.30
40q	200.53	−115.57	−316.10
41q, confA	199.19	−118.32	−317.51
41q, conf B	284.39	−120.96	−405.35
46	84.43	−82.77	−167.20
47	107.20	−68.53	−175.73

Extended Data Table 2 - Comparative energies of ligands bound to VatA and to the ribosome

Energies of **VM1**, **46**, and **47** bound to VatA or the *E. coli* ribosome, as evaluated by Prime with OPLS3e/VSGB2.1 after refinement with PHENIX-OPLS3e/VSGB2.1, where ligands are decoupled from the receptor environment. Included are VatA-bound **VM1** from 4HUS and *E. coli* ribosome-bound **VM1** from 4U25.

Compound	Ribosome	VatA chain	Energy (kcal/mol)
VM1	ASU 1		−58.27
VM1	ASU 2		−58.59
VM1		A	−58.52
47 (from **47**/**VS1**)	X		−65.51
47	X		−68.53
47		A	−67.99
47		B	−63.40
47		C	−68.13
47		D	−67.98
47		E	−62.18
47		F	−67.66

Compound	Ribosome	VatA chain	Energy (kcal/mol)
46 (from **46/VS1**)	X		−85.70
46	X		−82.77
46		A	−73.74
46		B	−79.70
46		C (conformer 1)	−67.31
46		C (conformer 2)	−65.70
46		D	−73.72
46		E	−69.07
46		F	−80.08

Extended Data Table 3.

Statistical analyses of mouse thigh *in vivo* data, MIC assays, and VatA kinetics data.

Analysis of the MIC data by Mann-Whitney U test, the murine thigh infection model data by One-way ANOVA followed by Tukey's test, and analysis of VatA in vitro acetylation kinetics data by two-tailed unpaired t-test and Cohen's d. MIC = minimum inhibitory concentration, CFU = colony forming units, M = mean, SD = standard deviation, SS = sum of squares, df = degrees of freedom, MS = mean square, Sign. = significance.

Mann-whitney U Test – MIC comparison of flopristin (4) and (47)

	N	MIC_{obs} (μg/mL)	M_{rank}	∑ rank	U	Z	p value
flopristin (**4**)	3	0.5, 0.5, 1.0	2	6	0	−1.9640	0.0248
47	3	8, 8, 8	5	15			* p < 0.05

One-way ANOVA- Murine thigh infection model comparison of flopristin (4), 47, and 24-hour control

			10 mg/kg					200 mg/kg		
Summary	**N**		$M_{log10\ CFU/thigh}$	$SD_{logl0\ CFU/thigh}$		**N**		$M_{log10\ CFU/thigh}$	$SD_{logl0\ CFU/thigh}$	
control	5		7.49	0.28		5		6.15	0.21	
flopristin (**4**)	5		5.93	0.28		5		5.25	0.31	
47	5		7.08	0.08		5		7.08	0.08	
total	15		6.83	0.72		15		6.16	0.80	
ANOVA	**SS**	***df***	**MS**	F_{ratio}	**Sign.**	**SS**	***df***	**MS**	F_{ratio}	**Sign.**
between groups	6.58	2	3.29	59.0	6.21e–7	8.35	2	4.18	86.3	7.53e–8
within groups	0.67	12	0.06			0.58	12	0.05		
total	7.25	14				8.94	14			
Tukey's Test	**Q statistic**		**p value**	**Inference**		**Q statistic**		**p value**	**Inference**	
4 vs control	3.93		0.041	* p < 0.05		9.41		0.001	** p < 0.01	

One-way ANOVA- Murine thigh infection model comparison of flopristin (4), 47, and 24-hour control

	10 mg/kg			200 mg/kg		
Summary	**N**	$M_{log10\ CFU/thigh}$	$SD_{logl0\ CFU/thigh}$	**N**	$M_{log10\ CFU/thigh}$	$SD_{logl0\ CFU/thigh}$
47 vs control	10.89	0.001	** p < 0.01	18.59	0.001	** p < 0.01
4 vs **47**	14.82	0.001	** p < 0.01	9.17	0.001	** p < 0.01

Two-tailed, unpaired t-test (Student's test) - *In vitro* acetylation of flopristin (4) and 47 by VatA

	N	$M_{kcat/Km}$	$SD_{kcat/Km}$	t	*df*	p value	Cohen's d
flopristin (**4**)	3	1.834	0.342	−4.391	4	0.012	3.585
47	3	0.765	0.247			* p < 0.05	

Supplementary Material

Refer to Web version on PubMed Central for supplementary material.

Acknowledgements

We thank Fred Ward and Jamie Cate for initial advice on ribosome purifications and translation assays, Eva Nogales and a UCSF-UCB Sackler Sabbatical Exchange Fellowship (J.S.F.) for initial cryo-EM access and training. A.A.T. and J.P. were supported by the National Science Foundation Graduate Research Fellowship Program under Grant No. 1650113. D.J.L. was supported by a Postdoctoral Individual National Research Award NIH AI148120. H.A.C. was supported by a National Institute on Minority Health and Health Disparities (NIMHD) research diversity supplement under NIH GM123159. This project was funded by the UCSF Program for Breakthrough Biomedical Research, funded in part by the Sandler Foundation (J.S.F. and I.B.S.), a Sangvhi-Agarwal Innovation Award (J.S.F.), Packard Fellowships from the David and Lucile Packard Foundation (J.S.F. and I.B.S.), NIH GM123159 (J.S.F.), and NIH GM128656 (I.B.S.). We thank George Meigs and James Holton at Beamline 8.3.1 at the Advanced Light Source, which is operated by the University of California Office of the President, Multicampus Research Programs and Initiatives grant MR-15-328599, the National Institutes of Health (R01 GM124149 and P30 GM124169), Plexxikon Inc., and the Integrated Diffraction Analysis Technologies program of the US Department of Energy Office of Biological and Environmental Research. The Advanced Light Source (Berkeley, CA) is a national user facility operated by Lawrence Berkeley National Laboratory on behalf of the US Department of Energy under contract number DE-AC02-05CH11231, Office of Basic Energy Sciences. We thank Michael Thompson for comments on the crystallography methods. We thank Alex Myasnikov and David Bulkley for technical support at the UCSF Center for Advanced CryoEM, which is supported by NIH grants S10OD020054 and S10OD021741 and the Howard Hughes Medical Institute (HHMI). We thank Ed Eng and Elina Kopylov for technical support at the National Center for CryoEM Access and Training (NCCAT) and the Simons Electron Microscopy Center located at the New York Structural Biology Center, which is supported by the NIH Common Fund Transformative High Resolution Cryo-Electron Microscopy program (U24 GM129539) and by grants from the Simons Foundation (SF349247) and NY State. We thank William Weiss at the University of North Texas Health Science Center for conducting the animal study.

References

1. Wright PM, Seiple IB & Myers AG The evolving role of chemical synthesis in antibacterial drug discovery. Angew. Chem. Int. Ed Engl 53, 8840–8869 (2014). [PubMed: 24990531]
2. Stogios PJ et al. Potential for reduction of streptogramin A resistance revealed by structural analysis of acetyltransferase VatA. Antimicrob. Agents Chemother 58, 7083–7092 (2014). [PubMed: 25223995]
3. Vazquez D. The Streptogramin Family of Antibiotics in Mechanism of Action (eds. Gottlieb D. & Shaw PD) 387–403 (Springer Berlin Heidelberg, 1967).
4. Waglechner N. & Wright GD Antibiotic resistance: it's bad, but why isn't it worse? BMC Biol. 15, 84 (2017). [PubMed: 28915805]

5. Seiple IB et al. A platform for the discovery of new macrolide antibiotics. Nature 533, 338–345 (2016). [PubMed: 27193679]
6. Charest MG, Lerner CD, Brubaker JD, Siegel DR & Myers AG A convergent enantioselective route to structurally diverse 6-deoxytetracycline antibiotics. Science 308, 395–398 (2005). [PubMed: 15831754]
7. Vidaillac C, Parra-Ruiz J, Winterfield P. & Rybak MJ In vitro pharmacokinetic/pharmacodynamic activity of NXL103 versus clindamycin and linezolid against clinical Staphylococcus aureus and Streptococcus pyogenes isolates. Int. J. Antimicrob. Agents 38, 301–306 (2011). [PubMed: 21764263]
8. Wilson DN The A-Z of bacterial translation inhibitors. Crit. Rev. Biochem. Mol. Biol 44, 393–433 (2009). [PubMed: 19929179]
9. Noeske J. et al. Synergy of streptogramin antibiotics occurs independently of their effects on translation. Antimicrob. Agents Chemother 58, 5269–5279 (2014). [PubMed: 24957822]
10. Hershberger E, Donabedian S, Konstantinou K. & Zervos MJ Quinupristin-dalfopristin resistance in gram-positive bacteria: mechanism of resistance and epidemiology. Clin. Infect. Dis 38, 92–98 (2004). [PubMed: 14679454]
11. Sharkey LKR & O'Neill AJ Antibiotic Resistance ABC-F Proteins: Bringing Target Protection into the Limelight. ACS Infect Dis 4, 239–246 (2018). [PubMed: 29376318]
12. Leclercq R. & Courvalin P. Bacterial resistance to macrolide, lincosamide, and streptogramin antibiotics by target modification. Antimicrob. Agents Chemother 35, 1267–1272 (1991). [PubMed: 1929280]
13. Haroche J. et al. Clonal diversity among streptogramin A-resistant Staphylococcus aureus isolates collected in French hospitals. J. Clin. Microbiol 41, 586–591 (2003). [PubMed: 12574251]
14. Werner G, Cuny C, Schmitz FJ & Witte W. Methicillin-resistant, quinupristin-dalfopristin-resistant Staphylococcus aureus with reduced sensitivity to glycopeptides. J. Clin. Microbiol 39, 3586–3590 (2001). [PubMed: 11574577]
15. Valour F. et al. Pristinamycin in the treatment of MSSA bone and joint infection. J. Antimicrob. Chemother 71, 1063–1070 (2016). [PubMed: 26801082]
16. Delgado G Jr, Neuhauser MM, Bearden DT & Danziger LH Quinupristin-dalfopristin: an overview. Pharmacotherapy: The Journal of Human Pharmacology and Drug Therapy 20, 1469–1485 (2000).
17. Politano AD & Sawyer RG NXL-103, a combination of flopristin and linopristin, for the potential treatment of bacterial infections including community-acquired pneumonia and MRSA. Curr. Opin. Investig. Drugs 11, 225–236 (2010).
18. Li Q. & Seiple IB Modular, Scalable Synthesis of Group A Streptogramin Antibiotics. J. Am. Chem. Soc 139, 13304–13307 (2017).
19. Li Q. & Seiple IB A concise route to virginiamycin M2. Tetrahedron 75, 3309–3318 (2019). [PubMed: 32764837]
20. Schlessinger RH & Li Y-J Total Synthesis of (−)-Virginiamycin M2 Using Second-Generation Vinylogous Urethane Chemistry. J. Am. Chem. Soc 118, 3301–3302 (1996).
21. Entwistle DA, Jordan SI, Montgomery J. & Pattenden G. Total synthesis of the virginiamycin antibiotic 14,15-anhydropristinamycin IIB. J. Chem. Soc. Perkin 1 1315–1317 (1996).
22. Tavares F, Lawson JP & Meyers AI Total Synthesis of Streptogramin Antibiotics. (−)-Madumycin II. J. Am. Chem. Soc 118, 3303–3304 (1996).
23. Ghosh AK & Liu W. A Convergent, Enantioselective Total Synthesis of Streptogramin Antibiotic (−)-Madumycin II. J. Org. Chem 62, 7908–7909 (1997). [PubMed: 11671887]
24. Breuilles P. & Uguen D. Total synthesis of pristinamycin IIB. Tetrahedron Lett. 39, 3149–3152 (1998).
25. Entwistle DA Total Synthesis of Oxazole-Based Virginiamycin Antibiotics: 14,15-Anhydropristinamycin IIB. Synthesis 1998, 603–612 (1998).
26. Dvorak CA et al. The Synthesis of Streptogramin Antibiotics:(−)-Griseoviridin and Its C-8 Epimer. Angew. Chem. Int. Ed 39, 1664–1666 (2000).

27. Wu J. & Panek JS Total synthesis of (−)-virginiamycin M2. Angew. Chem. Int. Ed Engl 49, 6165–6168 (2010). [PubMed: 20648503]
28. Wu J. & Panek JS Total synthesis of (−)-virginiamycin M2: application of crotylsilanes accessed by enantioselective Rh(II) or Cu(I) promoted carbenoid Si-H insertion. J. Org. Chem 76, 9900–9918 (2011). [PubMed: 22070230]
29. Afonine PV et al. Real-space refinement in PHENIX for cryo-EM and crystallography. Acta Crystallogr D Struct Biol 74, 531–544 (2018). [PubMed: 29872004]
30. Li J. et al. The VSGB 2.0 model: a next generation energy model for high resolution protein structure modeling. Proteins 79, 2794–2812 (2011). [PubMed: 21905107]
31. Harms JM, Schlünzen F, Fucini P, Bartels H. & Yonath A. Alterations at the peptidyl transferase centre of the ribosome induced by the synergistic action of the streptogramins dalfopristin and quinupristin. BMC Biol. 2, 4 (2004). [PubMed: 15059283]
32. Osterman IA et al. Madumycin II inhibits peptide bond formation by forcing the peptidyl transferase center into an inactive state. Nucleic Acids Res. 45, 7507–7514 (2017). [PubMed: 28505372]
33. Hansen JL, Moore PB & Steitz TA Structures of five antibiotics bound at the peptidyl transferase center of the large ribosomal subunit. J. Mol. Biol 330, 1061–1075 (2003). [PubMed: 12860128]
34. Tu D, Blaha G, Moore PB & Steitz TA Structures of MLSBK antibiotics bound to mutated large ribosomal subunits provide a structural explanation for resistance. Cell 121, 257–270 (2005). [PubMed: 15851032]
35. Hoang NH et al. Regio-selectively reduced streptogramin A analogue, 5,6-dihydrovirginiamycin M1 exhibits improved potency against MRSA. Lett. Appl. Microbiol 57, 393–398 (2013). [PubMed: 23815812]
36. Kingston DGI, Kolpak MX, LeFevre JW & Borup-Grochtmann I. Biosynthesis of antibiotics of the virginiamycin family. 3. Biosynthesis of virginiamycin M1. J. Am. Chem. Soc 105, 5106–5110 (1983).
37. Richter MF et al. Predictive compound accumulation rules yield a broad-spectrum antibiotic. Nature 545, 299–304 (2017). [PubMed: 28489819]
38. Sharkey LKR, Edwards TA & O'Neill AJ ABC-F Proteins Mediate Antibiotic Resistance through Ribosomal Protection. MBio 7, e01975 (2016).
39. CRBIP-Catalogue. https://catalogue-crbip.pasteur.fr/recherche_catalogue.xhtml.
40. Radika K. & Northrop DB Correlation of antibiotic resistance with Vmax/Km ratio of enzymatic modification of aminoglycosides by kanamycin acetyltransferase. Antimicrob. Agents Chemother 25, 479–482 (1984). [PubMed: 6375556]
41. Knies JL, Cai F. & Weinreich DM Enzyme Efficiency but Not Thermostability Drives Cefotaxime Resistance Evolution in TEM-1 β-Lactamase. Mol. Biol. Evol 34, 1040–1054 (2017). [PubMed: 28087769]
42. Polikanov YS, Steitz TA & Innis CA A proton wire to couple aminoacyl-tRNA accommodation and peptide-bond formation on the ribosome. Nat. Struct. Mol. Biol 21, 787–793 (2014). [PubMed: 25132179]
43. Renaud J-P et al. Cryo-EM in drug discovery: achievements, limitations and prospects. Nat. Rev. Drug Discov 17, 471–492 (2018). [PubMed: 29880918]
44. Wong W. et al. Mefloquine targets the Plasmodium falciparum 80S ribosome to inhibit protein synthesis. Nat Microbiol 2, 17031 (2017).
45. Llano-Sotelo B. et al. Binding and action of CEM-101, a new fluoroketolide antibiotic that inhibits protein synthesis. Antimicrob. Agents Chemother 54, 4961–4970 (2010). [PubMed: 20855725]

Extended Data References

46. Tropea JE, Cherry S. & Waugh DS Expression and purification of soluble His(6)-tagged TEV protease. Methods Mol. Biol 498, 297–307 (2009). [PubMed: 18988033]
47. Kuhn ML, Majorek KA, Minor W. & Anderson WF Broad-substrate screen as a tool to identify substrates for bacterial Gcn5-related N-acetyltransferases with unknown substrate specificity. Protein Sci. 22, 222–230 (2013). [PubMed: 23184347]

48. Winter G. xia2: an expert system for macromolecular crystallography data reduction. Journal of Applied Crystallography vol. 43 186–190 (2010).
49. Kabsch W. XDS. Acta Crystallogr. D Biol. Crystallogr 66, 125–132 (2010). [PubMed: 20124692]
50. Liebschner D. et al. Macromolecular structure determination using X-rays, neutrons and electrons: recent developments in Phenix. Acta Crystallogr D Struct Biol 75, 861–877 (2019). [PubMed: 31588918]
51. Emsley P, Lohkamp B, Scott WG & Cowtan K. Features and development of Coot. Acta Crystallogr. D Biol. Crystallogr 66, 486–501 (2010). [PubMed: 20383002]
52. Schuwirth BS et al. Structures of the bacterial ribosome at 3.5 A resolution. Science 310, 827–834 (2005). [PubMed: 16272117]
53. Passmore LA & Russo CJ Specimen Preparation for High-Resolution Cryo-EM. Methods Enzymol. 579, 51–86 (2016). [PubMed: 27572723]
54. Mastronarde DN Automated electron microscope tomography using robust prediction of specimen movements. J. Struct. Biol 152, 36–51 (2005). [PubMed: 16182563]
55. Suloway C. et al. Automated molecular microscopy: the new Leginon system. J. Struct. Biol 151, 41–60 (2005). [PubMed: 15890530]
56. Cheng A. et al. High resolution single particle cryo-electron microscopy using beam-image shift. J. Struct. Biol 204, 270–275 (2018). [PubMed: 30055234]
57. Zheng SQ et al. MotionCor2: anisotropic correction of beam-induced motion for improved cryo-electron microscopy. Nature Methods vol. 14 331–332 (2017). [PubMed: 28250466]
58. Grant T, Rohou A. & Grigorieff N. TEM, user-friendly software for single-particle image processing. Elife 7, (2018).
59. Pettersen EF et al. UCSF Chimera--a visualization system for exploratory research and analysis. J. Comput. Chem 25, 1605–1612 (2004). [PubMed: 15264254]
60. Noeske J. et al. High-resolution structure of the Escherichia coli ribosome. Nat. Struct. Mol. Biol 22, 336–341 (2015). [PubMed: 25775265]
61. Moriarty NW, Grosse-Kunstleve RW & Adams PD electronic Ligand Builder and Optimization Workbench (eLBOW): a tool for ligand coordinate and restraint generation. Acta Crystallogr. D Biol. Crystallogr 65, 1074–1080 (2009). [PubMed: 19770504]
62. Roos K. et al. OPLS3e: Extending Force Field Coverage for Drug-Like Small Molecules. J. Chem. Theory Comput 15, 1863–1874 (2019). [PubMed: 30768902]
63. Sindhikara D. et al. Improving Accuracy, Diversity, and Speed with Prime Macrocycle Conformational Sampling. J. Chem. Inf. Model 57, 1881–1894 (2017). [PubMed: 28727915]
64. Bochevarov AD et al. Jaguar: A high-performance quantum chemistry software program with strengths in life and materials sciences. International Journal of Quantum Chemistry vol. 113 2110–2142 (2013).

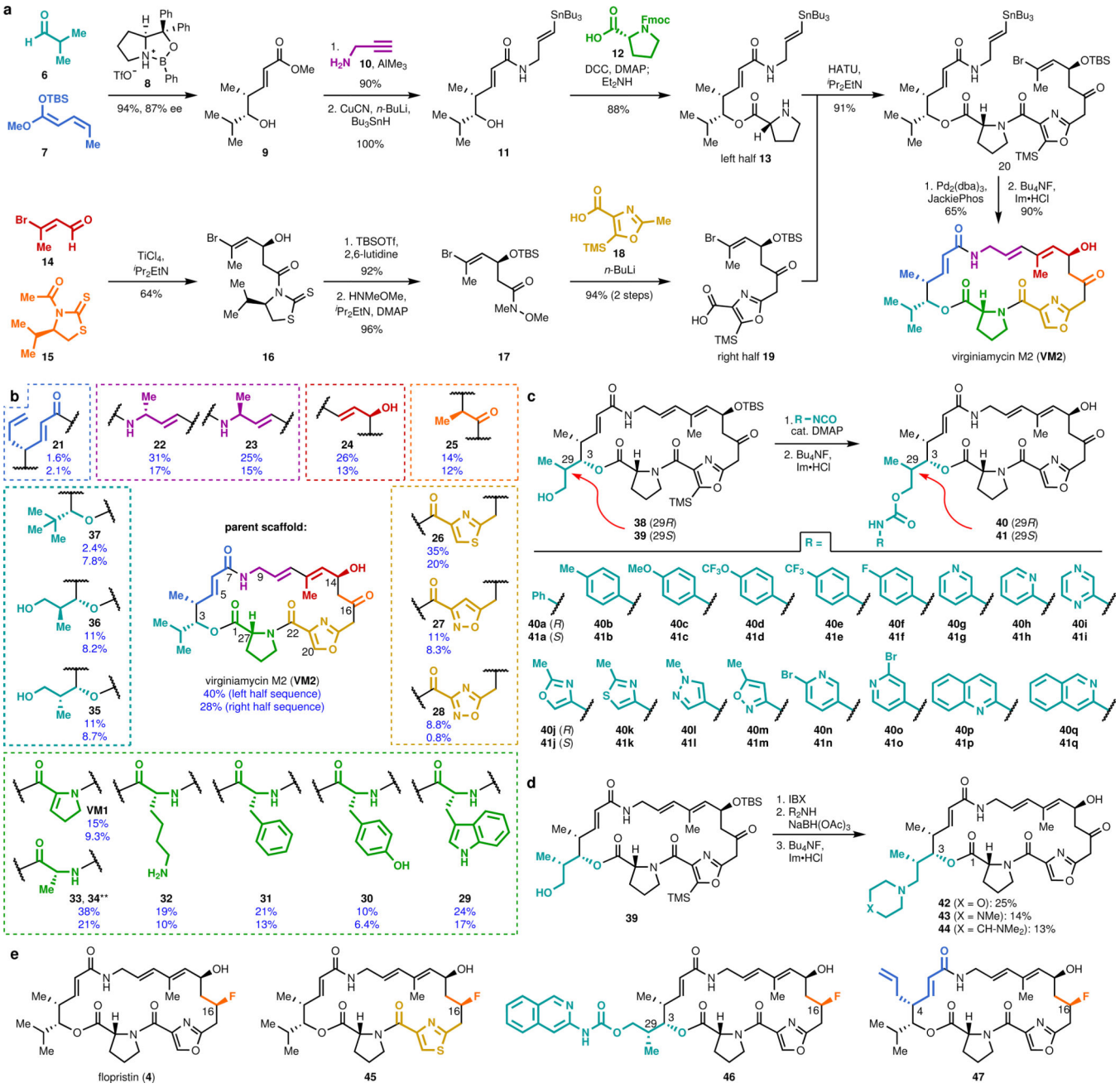

Figure 1 |. Modular synthesis enables access to >60 fully synthetic group A streptogramins.

a, Convergent route to **VM2** from seven building blocks. **b**, Eighteen group A streptogramins accessed by building block variation. The fragments displayed in the dashed boxes represent the structural variability compared to the parent scaffold (**VM2**). Overall yields for the synthesis of each analog for the left half sequence (top number) and for the right half sequence (bottom number) are displayed. ******Instead of a ketone, madumycin II (**34**) contains the following substitution at C16: α-H, β-OH. **c**, Access to 34 analogs (17 in each diastereomeric series) with C3 side chain variability by means of carbamate formation

followed by desilylation. **d**, Synthesis of tertiary-amine-containing analogs by oxidation and reductive amination. **e**, C16-fluorinated analogs.

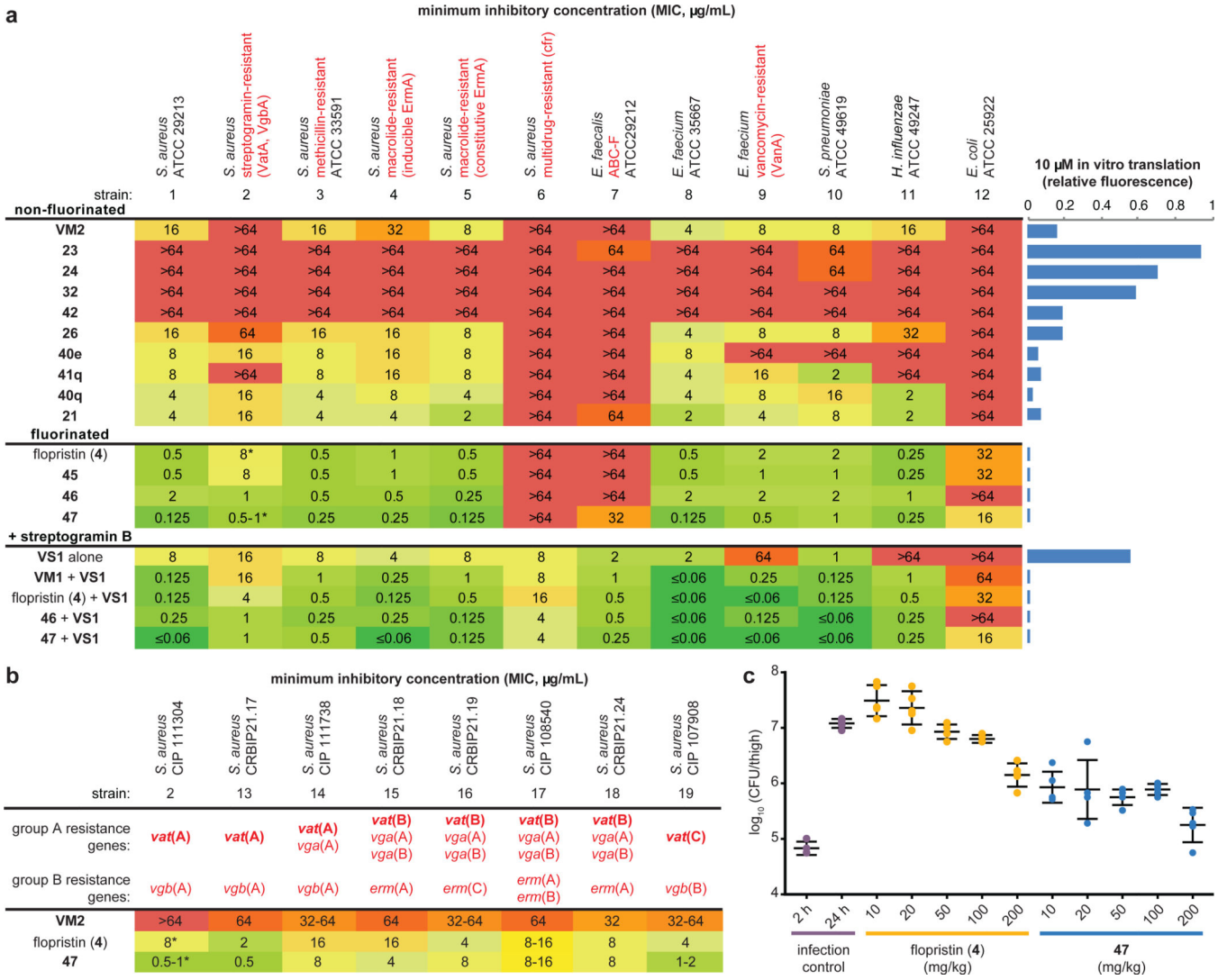

Figure 2 |. Antibiotic activity and *in vivo* efficacy of selected group A streptogramins.

a, MIC values for selected analogs against an expanded panel of pathogens. The bars to the right display *in vitro* translation that occurs in the presence of 10 μM of each analog (relative to DMSO). **b**, MIC values against eight clinical isolates of *S. aureus* with Vat resistance genes. The (*) indicates MIC values that were obtained in technical triplicate and biological triplicate. **c**, A murine thigh model of infection with *S. aureus* CIP 111304 (n=5 biologically independent animals per group, with the exception of the 2 h infection control where n=4 per group, examined over one experiment). Each animal is individually plotted, the center line is the mean, and the upper and lower whiskers bound the standard deviation from the mean. For detailed statistical analysis, see Extended Data Table 3.

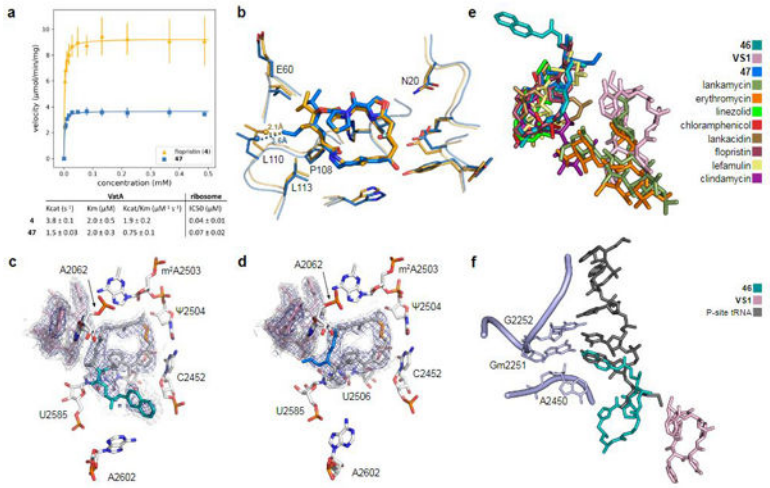

Figure 3 |. *In vitro* acetylation, VatA binding, and ribosome binding of highly active analogs. **a,** Summary of VatA acetylation kinetics and *in vitro* inhibition of the *E. coli* ribosome by **4** and **47**. Error bars represent standard deviations of the mean (3 technical replicates). For detailed statistical analysis, see Extended Data Table 3. **b,** X-ray crystal structures of **VM1** bound to VatA (PDB ID: 4HUS, 2.4 Å) and **47** bound to VatA at 3.2 Å resolution. Distances shown are measured between carbons of the C4 extension of **47** and Leu110 in the **VM1**-bound VatA structure (in orange dashes, 2.1 Å) and in the **47**-bound VatA structure (in marine dashes, 3.6 Å). **c**, 2.7-Å cryo-EM Coulomb potential density map (contoured in dark blue at 4.0σ and light gray at 1.0σ) for ribosomes bound to **46** and **VS1**. **d,** 2.8-Å cryo-EM Coulomb potential density map for ribosomes bound to **47** and **VS1**. **e,** An overlay of known PTC-site antibiotics shows how the side chain of **46** and the extension of **47** occupy areas distinct to previously characterized antibiotics. **f,** Overlay of P-site tRNA (dark gray, PDB ID: 1VY4) with the cryo-EM structure of ribosome-bound **46** reveals that the sidechain extends into the P-site and mimics the terminal adenosine (A2450) of the tRNA.